Table 3 Differences in the prevalence of allergic diseases by sex (comparison between 1996 and 2006)

	1996		*P* value (univariate)	*P* value† (multivariate)	2006		*P* value (univariate)	*P* value† (multivariate)
	Male	Female			Male	Female		
	(*n* = 8,043)	(*n* = 8,036)			(*n* = 6,712)	(*n* = 6,482)		
BA	504 (6.3%)	320 (4.0%)	< 0.0001	< 0.0001	401 (6.0%)	260 (4.0%)	< 0.0001	< 0.0001
AD	304 (3.8%)	377 (4.7%)	0.004	< 0.0001	369 (5.5%)	364 (5.6%)	0.767	0.24
AR	1875 (23.3%)	1390 (17.3%)	< 0.0001	< 0.0001	2028 (30.2%)	1567 (24.2%)	< 0.0001	< 0.0001
AC	1064 (13.2%)	1087 (13.5%)	0.562	< 0.0001	1688 (25.1%)	1633 (25.2%)	0.961	0.001

† adjusted for age, birth order, family history of allergy and presense of other allergic diseases.

BA, bronchial asthma; AD, atopic dermatitis; AR, allergic rhinitis; AC, allergic conjunctivitis.

CHANGE IN THE SEX DIFFERENCE IN THE PREVALENCE OF ALLERGIC DISEASES

In accordance with previous reports,[23] a significant male predominance in the prevalence of BA and AR in both 1996 and 2006 was found (Table 3). Interestingly, however, the female predominance in the prevalence of AD observed in 1996, disappeared, and no sex differences were observed in 2006. This indicates the increased prevalence of AD particularly among boys during the 10-year period (Table 3).

DISCUSSION

In this study, we set out to determine the changes in the recent trends seen in the childhood allergy epidemic in Japan. Using the same questionnaire and targeting the same population of schoolchildren in the corresponding area, we found that the prevalence of BA had reached a plateau, while that of AD, AR, and AC increased from 1996 to 2006. The results are in line with the Japanese data reported as part of the ISAAC survey of worldwide trends in the prevalence of allergic diseases,[4,24] in which the prevalence of BA plateaued or decreased, while that of AR and ARC increased in the last 8 years. The data were further examined by evaluating the changes in severity, past history, and sex ratio for each disease.

No significant changes in BA prevalence have been found during the past 10 years. Moreover, there was a statistically significant reduction in the distribution of severe cases. There was no change in the sex ratio, with a higher prevalence in boys than in girls. Meanwhile, those with a past history of BA increased, and lifetime prevalence increased significantly. Given that a past history was defined as the existence of BA symptoms beyond the 2 most recent years, these results may indicate that the BA symptoms were better controlled during the 10-year period, probably due to improved long-term management plans and their spread among general practitioners. However, it is still uncertain whether those with a past history were actually cured or their symptoms had ceased due to medication, such as inhaled corticosteroids and/or leukotriene receptor antagonists. In fact, in children at high risk for asthma, 2 years of inhaled corticosteroid therapy showed no effect on the development of asthma symptoms during the following treatment-free year.[25] This issue cannot be evaluated in the present study because the questionnaire did not question the use of such antiasthmatic medications.

Both the prevalence and severity of AD increased significantly over the decade, which may reflect the chronic nature of the disease and no notable improvement in treatment strategies, despite progress in understanding the disease's basic mechanisms.[26] A deep-rooted tendency to avoid steroid ointments among Japanese due to excessive concern about side effects, may exaggerate the rising trend in AD. More effort in educating patients and caregivers with accurate knowledge about the disease and its treatment are necessary. It should be noted that the prevalence increased more in boys than in girls in the past 10 years, resulting in the disappearance of the female predominance seen in 1996. The same trend has been observed in 13- to 14-year-old children in England from 1996 to 2002.[6] Although the reason for this is not clear, one might speculate that boys are less conscious of their appearance and less adherent to skin care and treatment, which makes them more susceptible than girls to the environmental influences that increase AD symptoms.

Dramatic increases in the prevalence and severity of both AR and AC were also found. In particular, the prevalence of AC almost doubled, from 13.3% to 25.2% over the 10-year period, while the number with a past history of AC dropped, which indicates that AC-like "itchy eye" symptoms became more persistent. Strikingly, the prevalence of sJCP, defined as the presence of both AR and AC symptoms plus aggravation during the spring cedar pollen season, increased by 2.6 times, from 3.1% to 8.0%. The data suggests that part of the reason for the increase in AR and AC is the increase in JCP, formerly regarded as an adult disease, among children. The increase in JCP prevalence cannot be explained by the increase in the amount of pollen because the average amount of JC pollen was greater between 1994 and 1996 (3,330/cm^2/yr) than between 2004 and 2006 (1,617/cm^2/yr) (data provided by the Kyoto Prefectural Pollen Information Center). The increase in JCP has become a serious social problem in Japan, and an increase in pediatric patients has also been noted in other reports.[27] On the other hand, the data should be carefully inter-

preted since JCP was not strictly defined in our questionnaire and overdiagnosis due to parents' increased awareness is possible, as those with both AR and AC who experienced aggravated symptoms during the spring season were regarded as having "suspected" JCP. In addition, not only Japanese cedar but also Japanese cypress and sweet vernal grass are the major causes for pollinosis in the spring season in Japan. These issues urgently require more elucidation.

Our findings should be interpreted within the inherent limitations. That is, we used self-reported questionnaires to measure the prevalence of allergic diseases. Although previously attested questionnaires were used, some misclassification would be inevitable. However, such misclassification would result in both overestimation and underestimation. Therefore, we can conclude that the prevalence is still valid based on the large sample size.

In conclusion, although the prevalence of BA appears to have reached a plateau and its severity has improved, both the prevalence and the severity have increased for other allergic diseases, including AD, AR, and AC, from 1996 to 2006 in Kyoto, Japan, with the cumulative prevalence of BA still increasing. Overall, the results indicate there is still a rising trend in allergic diseases in Japanese schoolchildren. Based on the present results, more attention should be paid to skin and nasoocular symptoms which are increasing and becoming more aggravated. In order to develop better management and prevention strategies, it is also important to constantly monitor the changing trends in the prevalence of these diseases and to evaluate possible factors responsible for changes, such as alterations in lifestyle, environmental factors, and general awareness and management of symptoms.

ACKNOWLEDGEMENTS

We thank Dr. M. Yasuda of the Department of Otolaryngology, Head and Neck Surgery of Kyoto Prefectural University of Medicine, for providing the data on the pollen amount in Kyoto city. We also thank T. Yamaguchi for statistical assistance. This work was supported by Grants-in-Aid of the Ministry of Education, Culture, Sports, Science and Technology, Japan.

REFERENCES

1. Zöllner IK, Weiland SK, Piechotowski I *et al.* No increase in the prevalence of asthma, allergies, and atopic sensitization among children in Germany: 1992-2001. *Thorax* 2005;**60**:545-8.
2. Lee S-L, Wong W, Lau Y-L. Increasing prevalence of allergic rhinitis but not asthma among children in Hong Kong from 1995 to 2001 (Phase 3 International Study of Asthma and Allergies in Childhood). *Pediatr Allergy Immunol* 2004;**15**:72-8.
3. Williams H, Stewart A, von Mutius E, Cookson W, Anderson HR. Is eczema really on the increase worldwide? *J Allergy Clin Immunol* 2008;**121**:947-54.
4. Asher MI, Montefort S, Björkstén B *et al.* Worldwide time trends in the prevalence of symptoms of asthma, allergic rhinoconjunctivitis, and eczema in childhood: ISAAC phases one and three repeat multicountry cross-sectional surveys. *Lancet* 2006;**368**:733-43.
5. Maziak W, Behrens T, Brasky TM *et al.* Are asthma and allergies in children and adolescents increasing? Results from ISAAC phase I and phase III surveys in Münster, Germany. *Allergy* 2003;**58**:572-9.
6. Shamssain M. Trends in the prevalence and severity of asthma, rhinitis and atopic eczema in 6- to 7- and 13- to 14-yr-old children from the north-east of England. *Pediatr Allergy Immunol* 2007;**18**:149-53.
7. Schernhammer ES, Vutuc C, Waldhör T, Haidinger G. Time trends of the prevalence of asthma and allergic disease in Austrian children. *Pediatr Allergy Immunol* 2008; **19**:125-31.
8. Anderson HR, Ruggles R, Strachan DP *et al.* Trends in prevalence of symptoms of asthma, hay fever, and eczema in 12-14 year olds in the British Isles, 1995-2002: questionnaire survey. *BMJ* 2004;**328**:1052-3.
9. Braun-Fahrländer C, Gassner M, Grize L *et al.* No further increase in asthma, hay fever and atopic sensitization in adolescents living in Switzerland. *Eur Respir J* 2004;**23**: 407-13.
10. Wong GW, Leung TF, Ko FW *et al.* Declining asthma prevalence in Hong Kong Chinese schoolchildren. *Clin Exp Allergy* 2004;**34**:1550-5.
11. Wang XS, Tan TN, Shek LP *et al.* The prevalence of asthma and allergies in Singapore; data from two ISAAC surveys seven years apart. *Arch Dis Child* 2004;**89**:423-6.
12. Graca-Marcos L, Quirs AB, Hernandez GG *et al.* Stabilization of asthma prevalence among adolescents and increase among schoolchildren (ISAAC phases I and III) in Spain. *Allergy* 2004;**59**:1301-7.
13. Riedi CA, Rosario NA, Ribas LF *et al.* Increase in prevalence of rhinoconjunctivitis but not asthma and atopic eczema in teenagers. *J Investig Allergol Clin Immunol* 2005; **15**:183-8.
14. Annus T, Riikjärv MA, Rahu K, Björksten B. Modest increase in seasonal allergic rhinitis and eczema over 8 years among Estonian schoolchildren. *Pediatr Allergy Immunol* 2005;**16**:315-20.
15. Selnes A, Nystad W, Bolle R, Lund E. Diverging prevalence trends of atopic disorders in Norwegian children. Results from three cross-sectional studies. *Allergy* 2005; **60**:894-9.
16. Grize L, Gassner M, Wüthrich B *et al.* Trends in prevalence of asthma, allergic rhinitis and atopic dermatitis in 5-7-year old Swiss children from 1992 to 2001. *Allergy* 2006;**61**:556-62.
17. Nishima S, Chisaka H, Fujiwara T *et al.* Surveys on the prevalence of pediatric bronchial asthma in Japan: a comparison between the 1982, 1992, and 2002 surveys conducted in the same region using the same methodology. *Allergol Int* 2009;**58**:37-53.
18. Odajima H, Nishima S. [Asthma prevalence survey in Fukuoka city]. *[Jap J Pediatr Allergy Clin Immunol]* 2007; **21**:739-42(in Japanese).
19. Kusunoki T, Asai K, Harazaki M, Korematsu S, Hosoi S. Month of birth and prevalence of atopic dermatitis in schoolchildren: dry skin in early infancy as a possible etiologic factor. *J Allergy Clin Immunol* 1999;**103**:1148-52.
20. The International Study of Asthma and Allergies in Childhood (ISAAC) Steering Committee. Worldwide variation in prevalence of symptoms of asthma, allergic rhinocon-

junctivitis, and atopic eczema: ISAAC. *Lancet* 1998;**351**: 1225-32.
21. Hosoi S, Asai K, Harazaki T, Furusho K, Mikawa H. [A epidemiologic study on the prevalence of the allergic diseases in school children in Kyoto city]. *Arerugi* 1997;**46**: 1025-35 (in Japanese).
22. Kusunoki T, Morimoto T, Nishikomori R *et al.* Obesity and the prevalence of allergic diseases in schoolchildren. *Pediatr Allergy Immunol* 2008;**19**:527-34.
23. Bacharier LB, Strunk RC. Asthma in older children. In: Leung DYM, Sampson HA, Geha RS, Szefler SJ (eds). *Pediatric Allergy: Principles and Practice.* St.Louis, Missouri: Mosby, 2003;405-24.
24. Björkstén B, Clayton T, Ellwood P, Stewart A, Strachan D. Worldwide time trends for symptoms of rhinitis and conjunctivitis: phase III of the International Study of Asthma and Allergies in Childhood. *Pediatr Allergy Immunol* 2008;**19**:110-24.
25. Guilbert TW, Morgan WJ, Zeiger RS *et al.* Long-term inhaled corticosteroids in preschool children at high risk for asthma. *N Engl J Med* 2006;**354**:1985-97.
26. Elias PM, Hatano Y, Williams ML. Basis for the barrier abnormality in atopic dermatitis: outside-inside-outside pathogenic mechanisms. *J Allergy Clin Immunol* 2008; **121**:1337-43.
27. Kimura M, Obi M, Saito M. Japanese cedar-pollen-specific IL-5 production in infants with atopic dermatitis. *Int Arch Allergy Immunol* 2004;**135**:343-7.

Virology 394 (2009) 64–72

Contents lists available at ScienceDirect

Virology

journal homepage: www.elsevier.com/locate/yviro

Selective infection of CD4$^+$ effector memory T lymphocytes leads to preferential depletion of memory T lymphocytes in R5 HIV-1-infected humanized NOD/SCID/IL-2Rγ^{null} mice

Chuanyi Nie [a,1], Kei Sato [a,1], Naoko Misawa [a], Hiroko Kitayama [a], Hisanori Fujino [b], Hidefumi Hiramatsu [b], Toshio Heike [b], Tatsutoshi Nakahata [b], Yuetsu Tanaka [c], Mamoru Ito [d], Yoshio Koyanagi [a,*]

[a] Laboratory of Viral Pathogenesis, Institute for Virus Research, Kyoto University, 53 Shogoinkawara-cho, Sakyo-ku, Kyoto, Kyoto 606-8507, Japan
[b] Department of Pediatrics, Graduate School of Medicine, Kyoto University, Kyoto, Kyoto 606-8501, Japan
[c] Department of Immunology, Graduate School of Medicine, University of the Ryukyus, Nishihara, Okinawa 903-0125, Japan
[d] Central Institute for Experimental Animals, Kawasaki, Kanagawa 216-0001, Japan

ARTICLE INFO

Article history:
Received 8 April 2009
Returned to author for revision 19 July 2009
Accepted 4 August 2009
Available online 9 September 2009

Keywords:
HIV-1 pathogenesis
Humanized mouse
Memory cell depletion
Productive infection
T cell activation

ABSTRACT

To investigate the events leading to the depletion of CD4$^+$ T lymphocytes during long-term infection of human immunodeficiency virus type 1 (HIV-1), we infected human CD34$^+$ cells-transplanted NOD/SCID/IL-2Rγ^{null} mice with CXCR4-tropic and CCR5-tropic HIV-1. CXCR4-tropic HIV-1-infected mice were quickly depleted of CD4$^+$ thymocytes and both CD45RA$^+$ naïve and CD45RA$^-$ memory CD4$^+$ T lymphocytes, while CCR5-tropic HIV-1-infected mice were preferentially depleted of CD45RA$^-$ memory CD4$^+$ T lymphocytes. Staining of HIV-1 p24 antigen revealed that CCR5-tropic HIV-1 preferentially infected effector memory T lymphocytes (T_{EM}) rather than central memory T lymphocytes. In addition, the majority of p24$^+$ cells in CCR5-tropic HIV-1-infected mice were activated and in cycling phase. Taken together, our findings indicate that productive infection mainly takes place in the activated T_{EM} in cycling phase and further suggest that the predominant infection in T_{EM} would lead to the depletion of memory CD4$^+$ T lymphocytes in CCR5-tropic HIV-1-infected mice.

Introduction

While it is evident that human immunodeficiency virus type 1 (HIV-1) causes acquired immunodeficiency syndrome (AIDS) in humans, the mechanism by which HIV-1 accomplishes this remains unclear. The gradual loss of peripheral blood (PB) CD4$^+$ T lymphocytes during the asymptomatic phase of HIV-1 infection is one of the best prognostic predictors for the onset of AIDS (O'Brien et al., 1996), and CD4$^+$ T lymphocyte depletion is thought to be a serious pathological change in AIDS (McCune, 2001).

To define the mechanisms behind CD4$^+$ T lymphocyte depletion, a large number of studies have been conducted in humans, primates, and humanized mice by using HIV-1, simian immunodeficiency virus (SIV), and SIV/HIV-1 chimeric virus (SHIV) (Centlivre et al., 2007; Koyanagi et al., 2008; McCune, 2001). One of the important findings from previous studies was the dependence of pathogenesis on the co-receptor preference, CXCR4, and/or CCR5 (Berkowitz et al., 1998; Moore et al., 2004). CXCR4-tropic (X4) SHIV caused rapid and complete depletion of all subsets of CD4$^+$ T lymphocytes in rhesus macaques, which led to death from immunodeficiency (Nishimura et al., 2004). On the other hand, CCR5-tropic (R5) HIV-1 is the dominant type of HIV-1 found in patients, and clinical manifestation of HIV-1 infection resembles CCR5-tropic SIV infection (Berger, Murphy, and Farber, 1999). In both HIV-1-infected patients and SIV-infected rhesus macaques, the drastic onset of immunodeficiency is rare (Ambrose et al., 2007; McCune, 2001), and CD4$^+$ T lymphocytes in PB slowly decrease in number, eventually leading to immunodeficiency.

X4 virus uses CXCR4 as the co-receptor and R5 virus uses CCR5 as the co-receptor for viral infection into target cells (Berger, Murphy, and Farber, 1999; Lusso, 2006). CXCR4 is expressed on naïve T lymphocytes and thymocytes, thus X4 HIV-1 can infect naïve T lymphocytes and thymocytes (Pedroza-Martins et al., 1998). It is well known that faster depletion of immature thymocytes and T lymphocytes is observed after the appearance of X4 HIV-1 (Berkowitz et al., 1998; Pedroza-Martins et al., 1998; Schnittman et al., 1990). On the contrary, CCR5 is primarily expressed on CD4$^+$ effector memory T lymphocytes (T_{EM}) and macrophages but not on naïve and central memory CD4$^+$ T lymphocytes (T_{CM}) (Sallusto, Geginat, and Lanzavecchia, 2004). Therefore, the selective infection of T_{EM} is thought to leave naïve T lymphocytes and T_{CM} intact. Depletion of T_{EM} by R5 virus has been studied in SIV-infected rhesus macaques (Brenchley et al., 2004; Li et al., 2005). In 14–28 days following infection, the population of extra-lymphoid CCR5$^+$ T_{EM} was depleted up to 90% (Centlivre et al., 2007; Mattapallil et al., 2005; Okoye et al., 2007). At

* Corresponding author. Fax: +81 75 751 4812.
E-mail address: ykoyanag@virus.kyoto-u.ac.jp (Y. Koyanagi).
[1] These authors contributed equally to this study.

0042-6822/$ – see front matter © 2009 Elsevier Inc. All rights reserved.
doi:10.1016/j.virol.2009.08.011

the same time, an obvious reduction in $CD4^+$ T lymphocytes was not found in the PB. In an attempt to compensate for the loss of $CCR5^+$ T_{EM}, $CCR5^-$ T_{CM} was persistently activated and divided in order to prevent the collapse of the T_{EM} compartment (Brenchley, Price, and Douek, 2006). However, $CCR5^-$ T_{CM} lose their regenerative capability after prolonged period of proliferation, leading to decrease in both T_{CM} and T_{EM} compartments (Brenchley, Price, and Douek, 2006). This continuous shortage in $CCR5^+$ T_{EM} and accompanying $CCR5^-$ T_{CM} exhaustion are thought to play an important role in the progression to AIDS (Centlivre et al., 2007). Although the overloading of $CD4^+$ memory T lymphocyte homeostasis serves a compelling model of immunodeficiency in SIV infection, its relevance in HIV-1 infection is still poorly defined. Therefore, it is necessary that memory T lymphocyte infection is studied in an experimental animal model reconstituted with competent human immune cells.

To investigate the dynamics of $CD4^+$ T lymphocyte depletion following HIV-1 infection and the status of HIV-1-producing cells *in vivo*, we infected human $CD34^+$ cells-transplanted newborn NOG mice (NOG-hCD34 mice) with HIV-$1_{JR\text{-}CSF}$ (R5 HIV-1) or HIV-$1_{NL4\text{-}3}$ (X4 HIV-1). Our findings indicate that X4 HIV-1 infection can cause the depletion of $CD4^+$ thymocytes which results in the reduction in both naïve and memory T lymphocytes, while R5 HIV-1 infection can selectively deplete memory $CD4^+$ T lymphocytes. Further analyses indicate that R5 HIV-1 preferentially infects $CCR7^-$ T_{EM} and that the infected cells are predominantly activated and in an actively proliferating state. These results suggest that preferential infection in the activated T_{EM} leads to selective depletion of memory $CD4^+$ T lymphocytes in R5 HIV-1-infected patients.

Results

Kinetics of PB $CD4^+$ T lymphocyte depletion in R5 and X4 HIV-1-infected mice

NOG-hCD34 mice were generated by human $CD34^+$ hematopoietic stem cell transplantation into neonatal NOG mice as described previously (Baenziger et al., 2006; Traggiai et al., 2004). A significant level of human leukocytes was maintained in the whole PB of 13–44

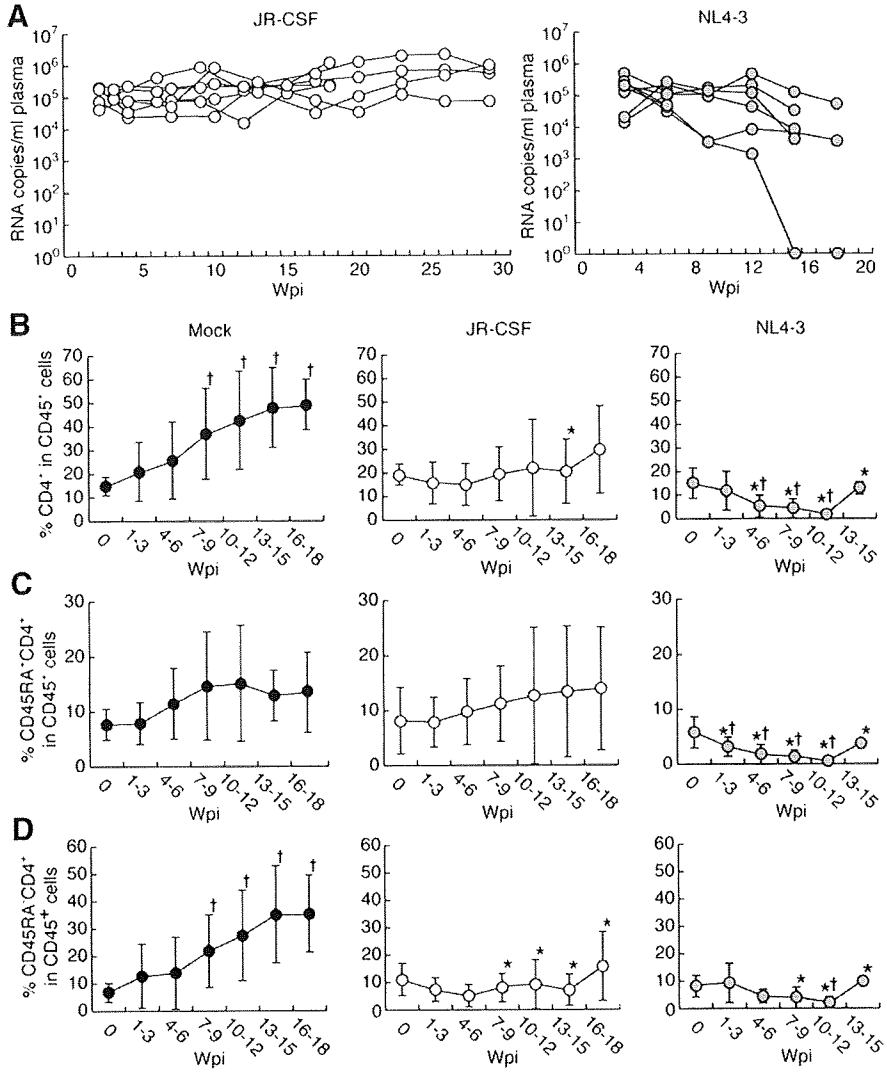

Fig. 1. Longitudinal analysis on plasma viral load and $CD4^+$ T lymphocytes in the PB of R5 and X4 HIV-1-infected mice. NOG-hCD34 mice were intraperitoneally injected with 1×10^5 $TCID_{50}$ of HIV-$1_{JR\text{-}CSF}$ ($n=7$) or HIV-$1_{NL4\text{-}3}$ ($n=8$) between 12 and 13 weeks olds. (A) The longitudinal analysis on the plasma viral load of HIV-$1_{JR\text{-}CSF}$-infected (left) and HIV-$1_{NL4\text{-}3}$-infected (right) mice. (B–D) PB was routinely sampled and analyzed for CD45RA expression in $CD4^+$ T lymphocytes from mock-infected ($n=8$), HIV-$1_{JR\text{-}CSF}$-infected ($n=7$), and HIV-$1_{NL4\text{-}3}$-infected ($n=8$) mice. We assigned data into 7 periodic groups (data taken at 0, between 1–3, 4–6, 7–9, 10–12, 13–15, and 16–18 wpi), and the average percentage and standard deviation were calculated using data obtained from each mouse during each time period. The percentages of $CD4^+$ (B), $CD45RA^+CD4^+$ (C), and $CD45RA^-CD4^+$ (D) T lymphocytes in the peripheral $CD45^+$ cells are shown. Error bars show standard deviations. Daggers represent statistical difference ($P<0.05$) when compared to the value at 0 wpi, and asterisks represent statistical difference when compared to the value obtained from the mock-infected mice.

week old mice (Supplemental Fig. 1A). Hematopoietic and lymphoid organs such as thymus, bone marrow, spleen and lymph nodes were highly repopulated with human mononuclear cells (Supplemental Figs. 1B–E). The expression of CCR5 was mainly restricted within the CD45RA$^-$ memory subset in CD4$^+$ T lymphocytes, and CXCR4 was broadly expressed on both naïve and memory T lymphocytes (Fig. 4C and data not shown) as observed in humans (Ebert and McColl, 2001).

NOG-hCD34 mice were inoculated with either an R5 HIV-1 (HIV-$1_{JR\text{-}CSF}$) or an X4 HIV-1 (HIV-$1_{NL4\text{-}3}$) between 12 and 13 weeks old. HIV-1 RNA was detected in the plasma of these mice as early as 3 weeks post-infection (wpi) and was maintained at high levels (1×10^4 to 10^6 copies per milliliter) until 28 wpi or until sacrificed (Fig. 1A). PB of these mice was then analyzed for longitudinal changes in CD4$^+$ T lymphocytes by flow cytometry. In the PB of both HIV-$1_{JR\text{-}CSF}$-infected and HIV-$1_{NL4\text{-}3}$-infected mice, depletion of human CD4$^+$ T lymphocytes was consistently found (Fig. 1B). In HIV-$1_{NL4\text{-}3}$-infected mice, both CD4$^+$CD45RA$^+$ naïve and CD4$^+$CD45RA$^-$ memory T lymphocytes were depleted, whereas in HIV-$1_{JR\text{-}CSF}$-infected mice, CD4$^+$CD45RA$^-$ memory T lymphocytes were specifically depleted (Figs. 1C and D). These data indicate that the infection with HIV-$1_{NL4\text{-}3}$ caused faster and more severe depletion of both naïve and memory subsets of CD4$^+$ T lymphocytes and the infection with HIV-$1_{JR\text{-}CSF}$ preferentially depleted memory CD4$^+$ T lymphocytes.

Thymopathy in X4 HIV-1-infected mice

To investigate the effect of HIV-1 infection on the thymopoiesis in NOG-hCD34 mice, the thymocytes from HIV-1-infected and mock-infected mice were isolated and were analyzed with flow cytometry. In mock-infected and HIV-$1_{JR\text{-}CSF}$-infected mice, CD4 and CD8 double positive (DP) thymocytes were predominant (Fig. 2A). CD4 single positive (SP) and CD8 SP thymocytes together made up a major fraction of the thymocyte population, and double negative (DN) thymocytes were only a minor fraction. In contrast, thymi from HIV-$1_{NL4\text{-}3}$-infected mice were severely depleted of both CD4 SP thymocytes and DP thymocytes (Figs. 2A–C). Furthermore, thymi from HIV-$1_{NL4\text{-}3}$-infected mice had greatly reduced number of all subsets of thymocytes (Fig. 2D). CD4 SP and DP thymocytes showed the greatest (approximately 100-fold) reduction, while CD8 SP thymocytes showed relatively milder (approximately 10-fold) reduction (Fig. 2D). These data indicate that infection with HIV-$1_{NL4\text{-}3}$ led to disturbed thymopoiesis and that HIV-$1_{JR\text{-}CSF}$ infection did not affect thymopoiesis.

Histological detection of p24-positive cells

HIV-1 p24-positive cells productively produce HIV-1 virions. Since human CD45$^+$ mononuclear cells were very few or absent in HIV-$1_{NL4\text{-}3}$-infected mice when sacrificed, they were not further analyzed (data not shown). As presented in Fig. 3, the immunohistological staining showed the presence of HIV-1 p24-positive cells in all of the bone marrow, spleen, and lymph nodes. HIV-1 p24 staining co-localized with CD4 staining. Also, a larger percentage of cells seemed to be productively infected with HIV-1 in the spleen and lymph nodes.

Depletion of splenic memory CD4$^+$ T lymphocytes

We isolated mononuclear cells from the spleen of HIV-$1_{JR\text{-}CSF}$-infected and mock-infected mice and then analyzed them by flow cytometry. As shown in Fig. 4A, the percentage of CD4$^+$ T lymphocytes in the spleen of HIV-$1_{JR\text{-}CSF}$ mice was smaller than that of mock-infected mice by 2.7-fold ($P=0.003$), showing that HIV-$1_{JR\text{-}CSF}$-infected mice had significantly fewer splenic CD4$^+$ T lymphocytes. Moreover, the percentage of splenic CD4$^+$CD45RA$^-$ memory T lymphocytes in HIV-$1_{JR\text{-}CSF}$-infected mice was smaller than that in the mock-infected mice ($P=0.007$), whereas the percentages of splenic CD4$^+$CD45RA$^+$ naive T lymphocytes were indifferent ($P=0.17$) (Fig. 4B). In mock-infected mice, a significant fraction of CD4$^+$CD45RA$^-$ T lymphocytes were CCR5$^+$ memory T lymphocytes (Fig. 4C). In contrast, in HIV-$1_{JR\text{-}CSF}$-infected mice, we found approximately 20-fold reduction in the percentage (Fig. 4C) and 100-fold reduction in the number of CD4$^+$CD45RA$^-$CCR5$^+$ memory T lymphocytes (data not shown). These results suggest that the CCR5-expressing memory CD4$^+$ T lymphocytes are depleted by direct R5 HIV-1 infection and that such reduction of CCR5-expressing CD4$^+$ T lymphocytes would lead to the decrease in whole memory CD4$^+$ T lymphocytes.

Preferential HIV-1 productive infection in CD4-negative effector memory T lymphocytes

To characterize the immunophenotypes of HIV-1 productively infected cells in NOG-hCD34 mice, splenic mononuclear cells from

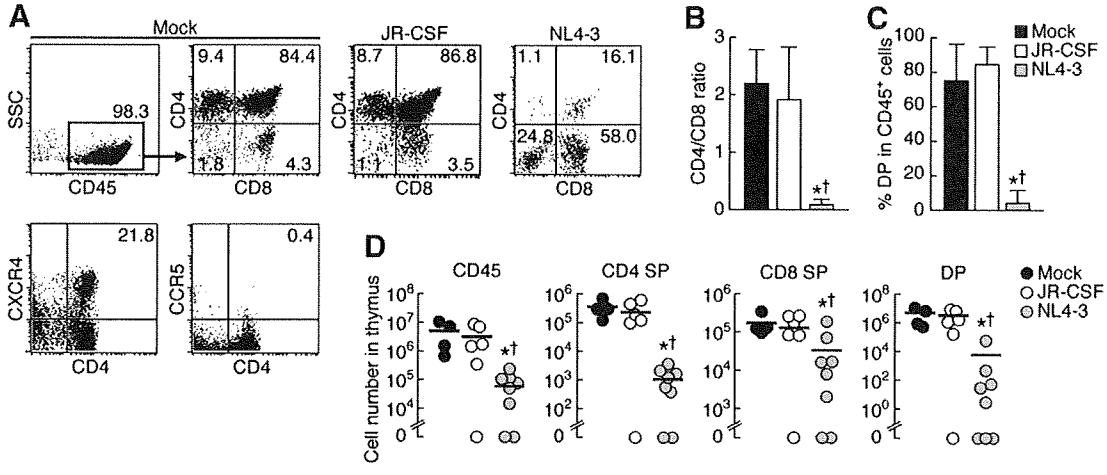

Fig. 2. Thymopathy in X4 HIV-1-infected mice. (A) Representative profile of flow cytometric analysis in thymi of mock-, HIV-$1_{JR\text{-}CSF}$-, and HIV-$1_{NL4\text{-}3}$-infected mice. The numbers in dot plots indicate the percentage of cells in CD45$^+$ thymocytes. (B and C) CD4/CD8 ratio (B) and the percentages of DP cells in CD45$^+$ thymocytes (C) in mock-infected ($n=4$), HIV-$1_{JR\text{-}CSF}$-infected ($n=5$), and HIV-$1_{NL4\text{-}3}$-infected ($n=6$) mice. (D) Number of CD45$^+$, CD4 SP, CD8 SP, and DP cells in thymi of mock-infected ($n=4$), HIV-$1_{JR\text{-}CSF}$-infected ($n=6$), and HIV-$1_{NL4\text{-}3}$-infected ($n=8$) mice. The horizontal bars in D show the average values, and the error bars in B and C show standard deviations. Asterisks indicate statistical significance ($P<0.05$) when compared to mock-infected mice, and daggers indicate statistical significance when compared to HIV-$1_{JR\text{-}CSF}$-infected mice.

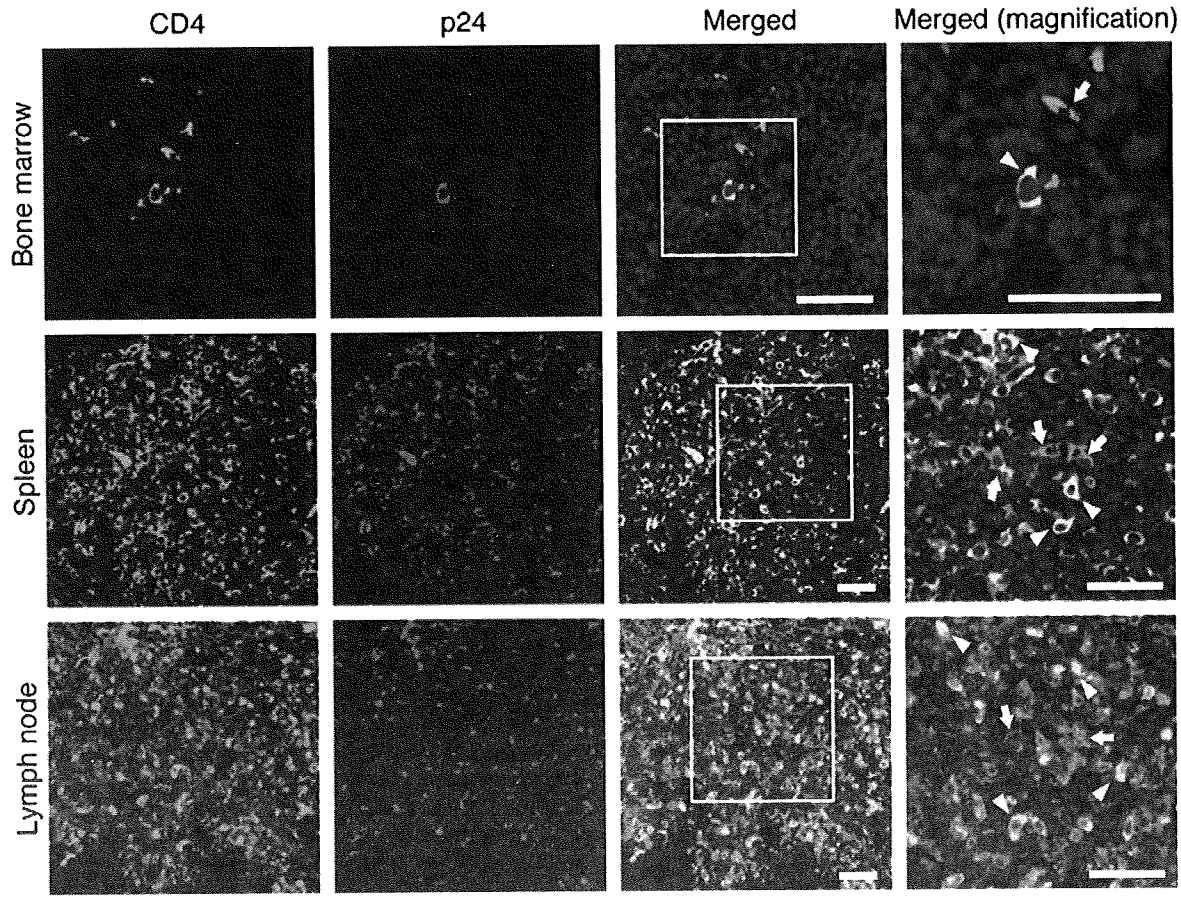

Fig. 3. Histological analysis on R5 HIV-1-infected mice. Representative immunohistological analysis of CD4 (green) and HIV-1 p24 (red) in the slices of bone marrow, spleen, and lymph nodes of HIV-$1_{JR\text{-}CSF}$-infected NOG-hCD34 mice. The low magnification images of the bone marrow slices were taken at ×80, and the high magnification images were taken at ×160. The low magnification images of the spleen and lymph nodes slices were taken at ×40, and the high magnification images were taken at ×80. The areas enclosed with the white squares were enlarged. The arrows point at representative $CD4^+$ cells and the arrowheads point at representative $CD4^+p24^+$ cells. Scale bars, 50 μm.

HIV-$1_{JR\text{-}CSF}$-infected mice were further analyzed for HIV-1 antigen p24 and the expression of lymphocyte surface markers. The anti-p24 antibody that we used did not react with any of the cells isolated from the mock-infected mice (Fig. 5A), as reported previously (Okuma et al., 2008). A significant fraction of splenic leukocytes expressed HIV-1 p24 and thus was productively infected with HIV-1 (Fig. 5A). The productively infected cells expressed surface CD3 but lacked surface CD4 (Figs. 5B and C). On average, over 90% of the $p24^+$ cells were $CD3^+$, yet only about 5% of these cells expressed surface CD4 (Fig. 5C). Also, p24-expressing cells were positive for CD45RO but not for CD45RA, suggesting that they were memory T lymphocytes ($73.7 \pm 24.3\%$ for $CD45RO^+CD45RA^-$ in $p24^+$ cells; Figs. 5D and E). Central memory T lymphocyte (T_{CM}) can be defined as a memory T lymphocyte that expresses CCR7, and effector memory T lymphocyte (T_{EM}) can be defined as a memory T lymphocyte that lacks CCR7 (Sallusto, Geginat, and Lanzavecchia, 2004). In p24-positive cells, $88.0 \pm 3.75\%$ was negative for CCR7 (Figs. 5D and F), suggesting that T_{EM} dominantly and productively infect with HIV-1.

Productive HIV-1 infection in activated and dividing lymphocytes

To investigate the activation status of the productively infected cells, splenic mononuclear cells were stained with anti-p24, anti-Ki67, and anti-CD69 antibodies. Ki67 antigen is exclusively expressed in proliferating cells, and CD69 is expressed on the surface of the activated cells at the early phase (Sereti et al., 2007; Vatakis et al., 2007). In splenic $CD4^+$ T lymphocytes from mock-infected mice or p24-negative splenocytes from HIV-$1_{JR\text{-}CSF}$-infected mice, only a minor fraction of the cells expressed either Ki67 or CD69 (Figs. 6A and B). In contrast, the majority of p24-positive splenocytes from HIV-$1_{JR\text{-}CSF}$-infected mice expressed Ki67 and/or CD69 (Figs. 6A and B). Also, the percentage of cells positive for both Ki67 and CD69 were higher in p24-positive cells than in p24-negative splenocytes from HIV-$1_{JR\text{-}CSF}$-infected mice and in splenic $CD4^+$ T lymphocytes from mock-infected mice (Fig. 6B). These results indicate that a significantly higher frequency of p24-positive cells is activated and/or proliferating cells. Notably, although the frequency was significantly low, we could detect $Ki67^-CD69^-$ resting T lymphocytes in p24-positive cells (Figs. 6A and B).

To further analyze the cell cycle of HIV-1 productively infected cells (i.e., p24-positive cells), we carried out Hoechst staining, which quantifies DNA content of the cells. Ki67 staining in combination with the Hoechst staining will sort cells into those in G_0/G_{1a}, G_{1b}, and $S/G_2/M$ phases of the cell cycle (Wilpshaar et al., 2000). As shown in Fig. 6C, non-stimulated human peripheral blood leukocytes (PBLs) predominantly exist in G_0/G_{1a} phases ($Ki67^-Hoechst^{low}$, lower left in the quadrant), while PHA-activated human PBLs predominantly exist in cycling G_{1b} phase ($Ki67^+Hoechst^{low}$, upper left in the quadrant) and $S/G_2/M$ phases ($Ki67^+Hoechst^{high}$, upper right in the quadrant). By using this method, we observed that p24-positive cells contained a significantly higher frequency of cells in the G_{1b} phase. In addition, the percentage of p24-positive cells in $S/G_2/M$ phases was significantly higher than $CD4^+$ splenocytes from mock-infected mice (Figs. 6D and E). These findings indicate that the majority of HIV-1-producing cells in the spleen of R5 HIV-1-infected mice are activated and in cycling phase. On the other hand, we detected the p24-

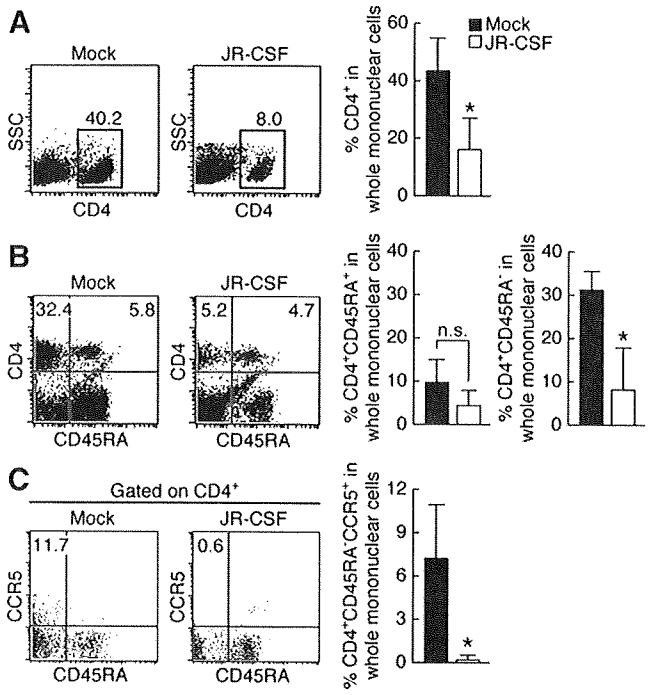

Fig. 4. The effect of R5 HIV-1 infection on the splenic CD4$^+$ T lymphocyte population. (A–C) Staining of splenic nucleated cells from the spleen of mock-infected ($n=4$) and HIV-$1_{JR\text{-}CSF}$-infected ($n=4$) mice were stained with CD4 (A), CD4 and CD45RA (B), and CCR5, CD4, and CD45RA (C). Representative profiles are shown, and the numbers in dot plots indicate the percentage of cells in CD45$^+$ splenic human leukocytes (A and B) or in CD4$^+$ cells (C). The graphs show the percentages of cells possessing each phenotype in whole mononuclear cells. The error bars show standard deviations. Asterisks indicate statistical significance ($P<0.05$) when compared to mock-infected mice.

positive splenocytes in G_0/G_{1a} phases, although the frequency was significantly lower than p24-negative splenocytes or CD4$^+$ splenocytes from mock-infected mice (Figs. 6D and E). These data suggest that a fraction of resting cells productively infects HIV-1. Moreover, we detected the significantly higher percentage of cells in $S/G_2/M$ phases in splenic p24-negative cells of HIV-$1_{JR\text{-}CSF}$-infected mice when comparing to that in splenic CD4$^+$ T lymphocytes of mock-infected mice (Figs. 6D and E).

Discussion

To investigate the mechanisms of CD4$^+$ T lymphocyte depletion by HIV-1 infection, we utilize human CD34$^+$ cells-transplanted NOG mice (Ito et al., 2002) and demonstrate that human CD4$^+$ T lymphocytes were differentially affected by X4 and R5 HIV-1 infection (Figs. 1–4). X4 virus induced immediate depletion of both naïve and memory CD4$^+$ T lymphocytes in periphery, while R5 virus gradually depleted memory CD4$^+$ T lymphocytes in the PB (Fig. 1) and spleen (Fig. 4). Our data suggest that distinctive pathogenesis of X4 and R5 viruses in NOG-hCD34 mice was caused by thymopathy (Fig. 2) and preferential infection of activated and dividing T_{EM} (Figs. 5 and 6), respectively. This is the first report addressing the mechanisms and dynamics of HIV-1-induced CD4$^+$ T lymphocyte depletion *in vivo*.

As previously shown in X4 SHIV-infected macaques (Ho et al., 2005; Nishimura et al., 2004), we observed the drastic loss of both naïve and memory T lymphocytes by X4 HIV-1-infected NOG-hCD34 mice (Fig. 1). We also found that CD4$^+$ thymocytes in NOG-hCD34 mice abundantly express CXCR4 (Fig. 2A) and that the CD4$^+$ thymocytes including DP and CD4 SP were preferentially reduced in HIV-$1_{NL4\text{-}3}$-infected mice (Fig. 2). It has been reported that intrathymic infection by X4 HIV-1 can lead to severe T lymphocytopenia (Berkowitz et al., 1998; Schnittman et al., 1990; Ye, Kirschner, and Kourtis, 2004). Therefore, our results suggest that the primary mechanism for naïve and memory T lymphocyte depletion in X4 virus infection can be attributed to impaired thymopoiesis caused by intrathymic infection.

In contrast to X4 HIV-1 infection, the depletion of PB CD4$^+$ T lymphocytes was more gradual and less intense in R5 HIV-1 infection and was confined to CD45RA$^-$ memory CD4$^+$ T lymphocytes (Fig. 1D). The selective depletion of memory CD4$^+$ T lymphocytes by R5 infection was also found in the spleen (Fig. 4). On the other hand, thymopathy was not detected in HIV-$1_{JR\text{-}CSF}$-infected mice (Fig. 2). These findings suggest that the selective depletion of memory CD4$^+$ T lymphocytes in PB and spleen of HIV-$1_{JR\text{-}CSF}$-infected mice caused through a different mechanism from HIV-$1_{NL4\text{-}3}$, and the mechanisms are further discussed below.

To investigate the mechanisms of memory CD4$^+$ T lymphocyte depletion in R5 HIV-1 infection in-depth, a series of flow cytometric analyses was carried out. The majority of p24$^+$ productively infected cells in the spleen were CD3$^+$ T lymphocytes (Figs. 5B and C). However, these infected cells were negative for surface CD4 (Figs. 5B

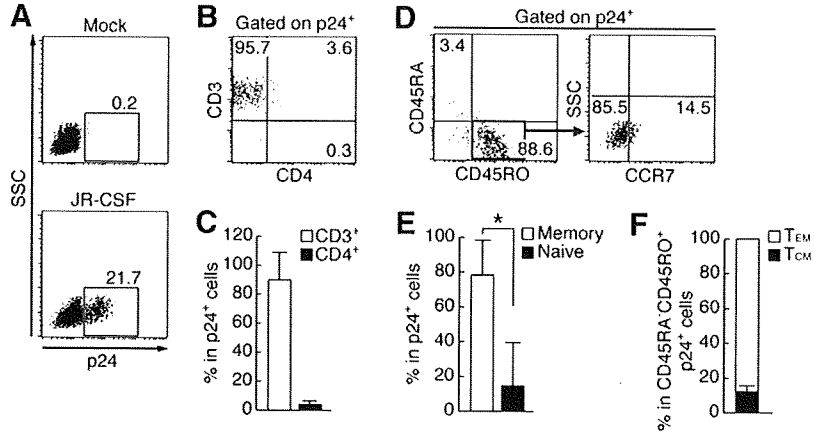

Fig. 5. Phenotype of productively infected p24$^+$ cells in the spleen of R5 HIV-1-infected mice. (A) Representative profiles of flow cytometric p24 staining in splenic nucleated cells of mock-infected ($n=4$) and HIV-$1_{JR\text{-}CSF}$-infected ($n=6$) mice. The numbers indicate the percentage of cells in splenic nucleated cells. (B and C) Staining of splenic nucleated cells of HIV-$1_{JR\text{-}CSF}$-infected mice for p24, CD3, and CD4. Representative profiles are shown in B, and the numbers in each quadrant indicate the percentage of cells in p24$^+$ cells. The percentages of each population in p24$^+$ cells are shown in C. (D–F) Staining of splenic nucleated cells of HIV-$1_{JR\text{-}CSF}$-infected mice for p24, CD45RA, CD45RO, and CCR7. Representative profiles are shown in D, and the numbers in each quadrant indicate the percentage of cells in p24$^+$ cells (left) or in p24$^+$CD45RA$^-$CD45RO$^+$ cells (right). The percentages of memory (CD45RA$^-$CD45RO$^+$) and naïve (CD45RA$^+$CD45RO$^-$) phenotyped cells in p24$^+$ cells are shown in E. The percentages of T_{EM} (CCR7$^-$CD45RA$^-$CD45RO$^+$) and T_{CM} (CCR7$^+$CD45RA$^-$CD45RO$^+$) in p24$^+$ cells are shown in F. The error bars in C, E, and F show standard deviations. Asterisks indicate statistical significance ($P<0.05$).

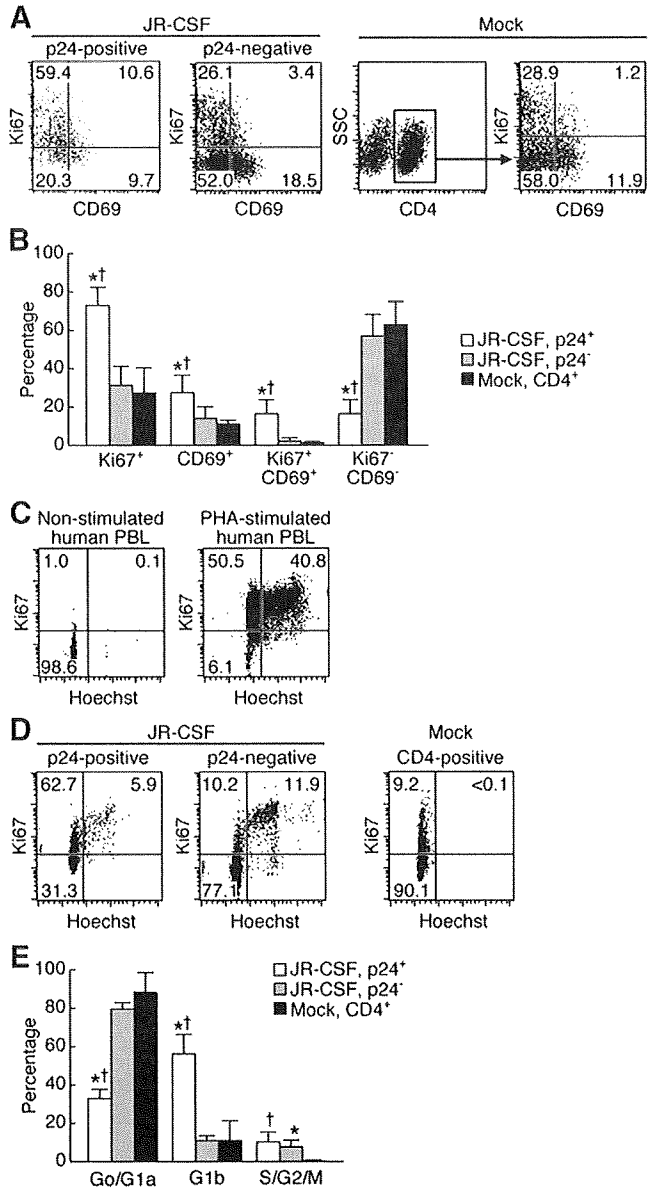

Fig. 6. Cell cycle analyses on productively infected $p24^+$ cells in the spleen of R5 HIV-1-infected mice. (A and B) Staining of splenic nucleated cells of mock-infected ($n=3$) and HIV-$1_{JR\text{-}CSF}$-infected ($n=4$) mice for Ki67, CD69, and either CD4 or p24. Representative profiles are shown in A, and each number indicates the percentage of cells in each quadrant. The graph in B shows the average percentages of cells possessing each population. (C) A representative profile of cell cycle analysis on non-stimulated human PBL (left panel) and PHA-activated human PBL (right panel) by using anti-Ki67 antibody and Hoechst. Each number indicates the percentage of cells in each quadrant. $Ki67^-Hoechst^{low}$ (lower left in quadrant) indicates G_0/G_{1a} phase, while $Ki67^+Hoechst^{low}$ (upper left in quadrant) and $Ki67^+Hoechst^{high}$ (upper right in quadrant) indicate G_{1b} and $S/G_2/M$ phases, respectively. (D and E) Staining of splenic nucleated cells of mock-infected mice ($n=4$) for CD4, Ki67, and Hoechst, and HIV-$1_{JR\text{-}CSF}$-infected mice ($n=4$) for p24, Ki67, and Hoechst. Representative profiles are shown in D, and each number indicates the percentage of cells in each quadrant. The graph in E shows the average percentages of cells in each population. The error bars in B and E show standard deviations. Asterisks indicate statistical significance ($P<0.05$) when compared to the value of p24-negative cells in HIV-$1_{JR\text{-}CSF}$-infected mice, and daggers indicate statistical significance when compared to the value of CD4-positive cells in mock-infected mice.

and C), although immunohistological analysis revealed that splenic $p24^+$ cells expressed CD4 molecules (Fig. 3). These results suggest that surface CD4 molecules are severely down-regulated following infection. In fact, it has been well documented that HIV-1 gene products such as *Nef* (Fackler, Alcover, and Schwartz, 2007; Roeth and Collins, 2006), *Env* (Crise, Buonocore, and Rose, 1990), and *Vpu* (Bour and Strebel, 2003; Geleziunas, Bour, and Wainberg, 1994) have the potential to down-regulate CD4 molecules from the surface of infected cells (Lindwasser, Chaudhuri, and Bonifacino, 2007). Similar down-regulation of surface CD4 has also been reported in lymph nodes and PB of HIV-1-infected patients (Cheney et al., 2006; Kaiser et al., 2007; Marodon et al., 1999). Therefore, this down-regulation of surface CD4 molecules in HIV-$1_{JR\text{-}CSF}$-infected mice is physiologically relevant and can play a role in the reduction of $CD4^+$ T lymphocytes.

In HIV-$1_{JR\text{-}CSF}$-infected mice, more than 80% of the productively infected cells were activated and in cycling phase (Fig. 6). It has been well known that activated cells massively produce HIV-1 virions (Ho et al., 1995). Therefore, this result suggests that the persistent viremia in R5 infection (Fig. 1A) is primarily due to the productive infection in the activated and proliferating cells. On the other hand, a fraction of infected cells were quiescent T lymphocytes negative for both activation and proliferation markers (Fig. 6). It is thought that HIV-1 cannot manifest productive infection in quiescent cells (Stevenson et al., 1990; Zack et al., 1990). However, studies on *ex vivo* infected human tonsil histocultures (Eckstein et al., 2001; Kinter et al., 2003), small intestines and cervix of SIV-infected rhesus macaques (Li et al., 2005; Zhang et al., 1999; Zhang et al., 2004), and HIV-1-infected patients (Zhang et al., 1999) have established that quiescent T lymphocytes residing in the lymphoid tissues are capable of supporting productive SIV or HIV-1 infection. Our results provide further support that productive infection of HIV-1 can take place in non-dividing cells, presumably resting T lymphocytes, in NOG-hCD34 mice. Productive infection not only in proliferative cells but also in quiescent cells may be an important factor in $CD4^+$ T lymphocyte depletion and persistent virus infection.

The preferential infection of $CD45RO^+CD45RA^-$ memory T lymphocytes with R5 HIV-1 is also the evidence supportive for the selective depletion of memory $CD4^+$ T lymphocytes (Figs. 5D and E). Nevertheless, only $16.3\pm9.7\%$ of splenic $CD4^+$ T lymphocytes expressed CCR5 in NOG-hCD34 mice, and the severe depletion of memory T lymphocytes in R5 HIV-1 infection cannot be explained by cell death caused by infection solely. In this regard, it has been reported that memory $CD4^+$ T lymphocyte reduction in SIV-infected macaques can be initiated by specific disruption of T_{EM} due to its preferential infection in the acute phase (Centlivre et al., 2007; Mattapallil et al., 2005; Okoye et al., 2007). In response to the T_{EM} reduction, T_{CM} proliferates and supplies *de novo* T_{EM} (Sallusto, Geginat, and Lanzavecchia, 2004). However, Brenchley et al. (2004) and Okoye et al. (2007) have reported that R5 virus infection induces chronic immune activation in macaques, which leads to the attenuation of regenerative capacity of T_{CM} (Brenchley et al., 2004; Okoye et al., 2007). In addition to the depletion of T_{EM} by direct infection, the attenuation of regenerative potential of T_{CM} causes not only the loss of T_{CM} but also the shortage of T_{EM} and eventually leads to the reduction of whole memory T lymphocytes (Brenchley et al., 2004; Okoye et al., 2007). This hypothesis of the dynamics of $CD4^+$ T lymphocyte depletion has been helpful for explaining the memory $CD4^+$ T lymphocyte in effector sites of SIV-infected macaques. Our observations in HIV-$1_{JR\text{-}CSF}$-infected mice, the severe depletion of memory T lymphocytes despite the limited availability of CCR5-expressing $CD4^+$ T lymphocytes and the preferential infection in T_{EM}, can be explained by the aforementioned hypothesis proposed in the previous literature (Brenchley et al., 2004; Okoye et al., 2007). Notably, we found that the frequency of cells in $S/G_2/M$ phases elevated in splenic p24-negative cells of HIV-$1_{JR\text{-}CSF}$-infected mice when comparing to that in splenic $CD4^+$ T lymphocytes of mock-infected mice (Figs. 6D and E). These data may explain that HIV-1 pathophysiology is caused by accelerated cells division, ultimately leading to the exhaustion of $CD4^+$ T lymphocytes. Taken together, our findings suggest that the selective infection of T_{EM} may be an important event that governs $CD4^+$ T lymphocyte depletion not

only in the effector sites of macaques during SIV infection but also in lymphoid organs during HIV-1 infection.

In summary, we showed differential $CD4^+$ T lymphocyte reduction in R5 and X4 HIV-1 infection. We report for the first time the selective depletion of memory $CD4^+$ T lymphocytes and the preferential infection of T_{EM} in an experimental model of R5 HIV-1 infection. Our data suggest that HIV-1 infection in T_{EM} can be an important step leading to $CD4^+$ T lymphocyte decline. Our findings confirm the applicability of NOG-hCD34 mice as a useful model to study the dynamics of HIV-1 pathogenesis including $CD4^+$ T lymphocytes depletion *in vivo*.

Materials and methods

Mice

NOD/SCID/IL-2Rγ^{null} (NOG) mice (Ito et al., 2002) were obtained from the Central Institute for Experimental Animals (Kanagawa, Japan). The mice were maintained under specific pathogen-free conditions and were handled in accordance with the Regulation on Animal Experimentation at Kyoto University.

Purification and transplantation of cord blood-derived CD34 cells

The purification of cord blood-derived CD34 cells was conducted as described previously (Ishikawa et al., 2005; Ito et al., 2002). Fresh human cord blood was obtained with parent written informed consent from healthy full-term newborns and CD34 MicroBead Kit (Miltenyi Biotec Inc, Auburn, CA) was used to isolate $hCD34^+$ cells according to the manufacturer's instructions. Cells were either stored at −80 °C or immediately transplanted when newborn mice were available. $CD34^+$ cells ($5–12\times10^4$) were intrahepatically injected into newborn mice of ages between 0 and 2 days after total radiation of 10 cGy per mouse in MBR-1520 x-ray irradiator (Hitachi Medico, Tokyo, Japan).

Peripheral blood collection and isolation of nucleated cells from organs

PB was routinely taken from NOG-hCD34 mice under ether anesthesia via retro-orbital venousplexus as described previously (Ishikawa et al., 2005). The red blood cells in the PB were lysed in preparation for flow cytometric analysis in 1× BD lysis buffer (BD Pharmingen, San Diego, CA). When the mice were sacrificed, PB was taken by cardiac puncture. Lymph nodes, thymi, spleen, and bone marrow were taken from HIV-1-infected and mock-infected mice upon sacrifice for histological or flow cytometric analysis. Lymph nodes and thymi were gently homogenized using a homogenizer pestle and spleens were crushed and rubbed on a steal mesh with 1-mm grids to generate single cell suspensions in RPMI 1640 supplemented with 4% fetal calf serum (FCS). To collect bone marrow, thigh bones were dissected at both ends and the interior was flushed with RPMI 1640 supplemented with 4% FCS. The cells were immediately used for flow cytometric analysis or stored in Cell Banker (Juji Field Inc., Tokyo, Japan) at −80 °C until use. As there are some variations in the combination of antibodies used to study the human cell population in each mouse, the number of data collected for each surface marker may differ. Data used for any longitudinal analysis were taken from identical mice.

Flow cytometric analysis of human blood cells in transplanted mice

The staining for flow cytometric analysis was done with some modifications to the protocol previously described (Sato et al., 2008). Briefly, for the surface staining, the cells were blocked with FcR blocker (Miltenyi Biotec Inc) for 5 min at room temperature (RT) and then incubated with the appropriate antibodies at optimum concentration in 1× phosphate-buffered saline (PBS) containing 2% FCS for 30 min at 4 °C. Fluorescein isothiocyanate-conjugated (FITC-conjugated) anti-human CD19 (HD37; Dako, Tokyo, Japan), CD8 (DK25; Dako), CD14 (TUK4; Miltenyi Biotec Inc), CD4 (L3T4; eBioscience, San Diego, CA), CD3 (UCHT1; BD Pharmingen, San Diego, CA), CCR5 (3A9; BD Pharmingen), and CD303/BDCA2 (AC144; Miltenyi Biotec Inc) mouse IgG monoclonal antibodies (mAb); phycoerythrin-conjugated anti-human CD3 (UCHT1; Dako), CD4 (MT310; Dako), CD34 (AC136; Miltenyi Biotec Inc), CD11c (B-ly6; BD Pharmingen), CXCR4 (12G5; BD Pharmingen), CCR7 (FAB197; R&D systems, Abingdon, UK), and CCR5 (3A9; BD Pharmingen) mouse IgG mAb; biotinylated anti-human CD45 (H130; eBioscience), CD45RA (HI-100; BD Pharmingen), CD8 (RPA-T8; BD Pharmingen), CD4 (RPA-T4; BD Pharmingen), and mouse IgG mAb; peridinin-chlorophyll-conjugated (PerCP-conjugated) anti-human CD69 (L78; BD Immunocytometry Systems, San Jose, CA) mouse IgG mAb; PE-Cy5-conjugated anti-human HLA-DR (G46-6; BD Pharmingen) mouse IgG mAb; allophycocyamin-conjugated anti-human CD45RO (UCHL1; BD Pharmingen) and CD8 (DK25; Dako) mouse IgG mAb were used. Each antibody was controlled with appropriate isotype antibodies purchased from Dako and BD Pharmingen. Streptavidin-PerCP (SA-PerCP) was purchased from BD Immunocytometry Systems. Following the incubation, the cells were washed and further incubated with SA-PerCP for 30 min at 4 °C, if needed. For the intracellular staining, the cells were permeabilized and fixed by treatment with BD Cytoperm/Cytofix solution (BD Pharmingen) and were stained with FITC-conjugated anti-HIV-1 p24 (clone 2C2) (Okuma et al., 2008) and anti-human Ki67 (B56; BD Pharmingen) mouse IgG mAb for 30 min at 4°C in 1× BD PermWash buffer (BD Pharmingen). For DNA staining to analyze cell cycle, the cells were incubated with Hoechst33342 (Invitrogen, Carlsbad, CA) for 30 min at 4 °C as described previously (Wilpshaar et al., 2000). Data collection was performed on BD FACSCan (BD Biosciences) for 3-color staining, BD FACSCalibur (BD Biosciences) for 4-color staining, and BD FACSCanto (BD Biosciences) for cell cycle analyses using Hoechst33342, and the obtained data were analyzed with CellQuest software (BD Immunocytometry System, San Jose, CA).

HIV-1 infection

NOG mice were injected intraperitoneally with RPMI 1640 ($n=8$) or 1×10^5 50% tissue culture infective doses ($TCID_{50}$) of $HIV\text{-}1_{JR\text{-}CSF}$ ($n=7$) or $HIV\text{-}1_{NL4\text{-}3}$ ($n=8$) between 12 and 13 weeks of ages. The viruses used were prepared by transfection as previously described (Sato et al., 2008). Infectious titers in the form of $TCID_{50}$ of each virus stock were determined by endpoint dilution with phytohemagglutinin-activated PBMCs as described (Koyanagi et al., 1997).

Detection of HIV-1 RNA in the plasma of infected mice

The detection of HIV-1 RNA in the plasma of the infected mice was routinely carried out using Amplicor HIV-1 monitor v1.5 according to the manufacturer's protocol (Roche Diagnostics, Mannheim, Germany).

Immunohistological analysis

Organs were fixed in 1× PBS containing 4% paraformalhyde and embedded in OCT compound (Sakura Finetechnical, Tokyo, Japan) after immersion in 10%–20% gradient sucrose. The OCT embedded organs were then sliced and were permeabilized with 0.1% Triton-X at RT for 10 min, incubated three times with 10 mM glycine for 5 min and blocked with 5% normal goat serum at RT for 1 hr. The sections were then incubated with mouse anti-HIV-1 p24 (Kal-1; Dako) IgG mAb at 4°C overnight, followed by incubation with Alexa Fluor 488-conjugated goat anti-mouse IgG (Invitrogen) at RT for 2 hr. The sections were further incubated with biotinylated mouse anti-

human CD4 IgG mAb (RFT-4g; Southern Biotech, Birmingham, AL) at 4°C overnight, followed by incubation with Streptavidin–Alexa Fluor 647 (Invitrogen) and Hoeschst33342 at RT for 2 hr. All the antibody staining was performed in blocking solution. Images were acquired with a Leica TCS SP2 AOBS confocal laser microscope (Leica Microsystems, Heidelberg, Germany).

Statistical analysis

Data were expressed as an average with standard deviation. Significant differences between data groups were determined by Student's *t* test or paired *t* test. A *P* value less than 0.05 was considered significantly different.

Acknowledgments

We would like to thank Peter Gee (Institute for Virus Research, Kyoto University) for proofreading of our manuscript and Munetada Haruyama (the Department of Pediatrics, Kyoto University) for their generous help in our study. We also would like to express our appreciation for Ms. Kotubu Misawa's dedicated support. This work was supported by a Grant-in-Aid for Scientific Research on Priority Areas from the Ministry of Education, Culture, Sports, Sciences, and Technology of Japan; a Health and Labour Science Research Grant (Research on Publicly Essential Drugs and Medical Devices) from the Ministry of Health, Labor and Welfare of Japan; and Japan Human Science Foundation. K.S. was supported by Research Fellowships of the Japan Society for the Promotion of Science for Young Scientists. Y. K. was supported by a grant from the Naito Foundation.

Appendix A. Supplementary data

Supplementary data associated with this article can be found, in the online version, at doi:10.1016/j.virol.2009.08.011.

References

Ambrose, Z., KewalRamani, V.N., Bieniasz, P.D., Hatziioannou, T., 2007. HIV/AIDS: in search of an animal model. Trends Biotechnol. 25, 333–337.

Baenziger, S., Tussiwand, R., Schlaepfer, E., Mazzucchelli, L., Heikenwalder, M., Kurrer, M.O., Behnke, S., Frey, J., Oxenius, A., Joller, H., Aguzzi, A., Manz, M.G., Speck, R.F., 2006. Disseminated and sustained HIV infection in $CD34^+$ cord blood cell-transplanted $Rag2^{-/-}\gamma_c^{-/-}$ mice. Proc. Natl. Acad. Sci. U. S. A. 103, 15951–15956.

Berger, E.A., Murphy, P.M., Farber, J.M., 1999. Chemokine receptors as HIV-1 coreceptors: roles in viral entry, tropism, and disease. Annu. Rev. Immunol. 17, 657–700.

Berkowitz, R.D., Alexander, S., Bare, C., Linquist-Stepps, V., Bogan, M., Moreno, M.E., Gibson, L., Wieder, E.D., Kosek, J., Stoddart, C.A., McCune, J.M., 1998. CCR5- and CXCR4-utilizing strains of human immunodeficiency virus type 1 exhibit differential tropism and pathogenesis *in vivo*. J. Virol. 72, 10108–10117.

Bour, S., Strebel, K., 2003. The HIV-1 Vpu protein: a multifunctional enhancer of viral particle release. Microbes. Infect. 5, 1029–1039.

Brenchley, J.M., Price, D.A., Douek, D.C., 2006. HIV disease: fallout from a mucosal catastrophe? Nat. Immunol. 7, 235–239.

Brenchley, J.M., Schacker, T.W., Ruff, L.E., Price, D.A., Taylor, J.H., Beilman, G.J., Nguyen, P.L., Khoruts, A., Larson, M., Haase, A.T., Douek, D.C., 2004. $CD4^+$ T cell depletion during all stages of HIV disease occurs predominantly in the gastrointestinal tract. J. Exp. Med. 200, 749–759.

Centlivre, M., Sala, M., Wain-Hobson, S., Berkhout, B., 2007. In HIV-1 pathogenesis the die is cast during primary infection. AIDS 21, 1–11.

Cheney, K.M., Kumar, R., Purins, A., Mundy, L., Ferguson, W., Shaw, D., Burrell, C.J., Li, P., 2006. HIV type 1 persistence in $CD4^-/CD8^-$ double negative T cells from patients on antiretroviral therapy. AIDS Res. Hum. Retroviruses 22, 66–75.

Crise, B., Buonocore, L., Rose, J.K., 1990. CD4 is retained in the endoplasmic reticulum by the human immunodeficiency virus type 1 glycoprotein precursor. J. Virol. 64, 5585–5593.

Ebert, L.M., McColl, S.R., 2001. Coregulation of CXC chemokine receptor and CD4 expression on T lymphocytes during allogeneic activation. J. Immunol. 166, 4870–4878.

Eckstein, D.A., Penn, M.L., Korin, Y.D., Scripture-Adams, D.D., Zack, J.A., Kreisberg, J.F., Roederer, M., Sherman, M.P., Chin, P.S., Goldsmith, M.A., 2001. HIV-1 actively replicates in naive $CD4^+$ T cells residing within human lymphoid tissues. Immunity 15, 671–682.

Fackler, O.T., Alcover, A., Schwartz, O., 2007. Modulation of the immunological synapse: a key to HIV-1 pathogenesis? Nat. Rev. Immunol. 7, 310–317.

Geleziunas, R., Bour, S., Wainberg, M.A., 1994. Cell surface down-modulation of CD4 after infection by HIV-1. FASEB J. 8, 593–600.

Ho, D.D., Neumann, A.U., Perelson, A.S., Chen, W., Leonard, J.M., Markowitz, M., 1995. Rapid turnover of plasma virions and CD4 lymphocytes in HIV-1 infection. Nature 373, 123–126.

Ho, S.H., Shek, L., Gettie, A., Blanchard, J., Cheng-Mayer, C., 2005. V3 loop-determined coreceptor preference dictates the dynamics of $CD4^+$-T-cell loss in simian–human immunodeficiency virus-infected macaques. J. Virol. 79, 12296–12303.

Ishikawa, F., Yasukawa, M., Lyons, B., Yoshida, S., Miyamoto, T., Yoshimoto, G., Watanabe, T., Akashi, K., Shultz, L.D., Harada, M., 2005. Development of functional human blood and immune systems in NOD/SCID/IL2 receptor γ $chain^{null}$ mice. Blood 106, 1565–1573.

Ito, M., Hiramatsu, H., Kobayashi, K., Suzue, K., Kawahata, M., Hioki, K., Ueyama, Y., Koyanagi, Y., Sugamura, K., Tsuji, K., Heike, T., Nakahata, T., 2002. NOD/SCID/γ_c^{null} mouse: an excellent recipient mouse model for engraftment of human cells. Blood 100, 3175–3182.

Kaiser, P., Joos, B., Niederost, B., Weber, R., Gunthard, H.F., Fischer, M., 2007. Productive human immunodeficiency virus type 1 infection in peripheral blood predominantly takes place in CD4/CD8 double-negative T lymphocytes. J. Virol. 81, 9693–9706.

Kinter, A., Moorthy, A., Jackson, R., Fauci, A.S., 2003. Productive HIV infection of resting $CD4^+$ T cells: role of lymphoid tissue microenvironment and effect of immunomodulating agents. AIDS Res. Hum. Retroviruses 19, 847–856.

Koyanagi, Y., Tanaka, Y., Ito, M., Yamamoto, N., 2008. Humanized mice for human retrovirus infection. Curr. Top Microbiol. Immunol. 324, 133–148.

Koyanagi, Y., Tanaka, Y., Kira, J., Ito, M., Hioki, K., Misawa, N., Kawano, Y., Yamasaki, K., Tanaka, R., Suzuki, Y., Ueyama, Y., Terada, E., Tanaka, T., Miyasaka, M., Kobayashi, T., Kumazawa, Y., Yamamoto, N., 1997. Primary human immunodeficiency virus type 1 viremia and central nervous system invasion in a novel hu-PBL-immunodeficient mouse strain. J. Virol. 71, 2417–2424.

Li, Q., Duan, L., Estes, J.D., Ma, Z.M., Rourke, T., Wang, Y., Reilly, C., Carlis, J., Miller, C.J., Haase, A.T., 2005. Peak SIV replication in resting memory $CD4^+$ T cells depletes gut lamina propria $CD4^+$ T cells. Nature 434, 1148–1152.

Lindwasser, O.W., Chaudhuri, R., Bonifacino, J.S., 2007. Mechanisms of CD4 downregulation by the Nef and Vpu proteins of primate immunodeficiency viruses. Curr. Mol. Med. 7, 171–184.

Lusso, P., 2006. HIV and the chemokine system: 10 years later. EMBO J. 25, 447–456.

Marodon, G., Warren, D., Filomio, M.C., Posnett, D.N., 1999. Productive infection of double-negative T cells with HIV *in vivo*. Proc. Natl. Acad. Sci. U. S. A. 96, 11958–11963.

Mattapallil, J.J., Douek, D.C., Hill, B., Nishimura, Y., Martin, M., Roederer, M., 2005. Massive infection and loss of memory $CD4^+$ T cells in multiple tissues during acute SIV infection. Nature 434, 1093–1097.

McCune, J.M., 2001. The dynamics of $CD4^+$ T-cell depletion in HIV disease. Nature 410, 974–979.

Moore, J.P., Kitchen, S.G., Pugach, P., Zack, J.A., 2004. The CCR5 and CXCR4 coreceptors – central to understanding the transmission and pathogenesis of human immunodeficiency virus type 1 infection. AIDS Res. Hum. Retroviruses 20, 111–126.

Nishimura, Y., Igarashi, T., Donau, O.K., Buckler-White, A., Buckler, C., Lafont, B.A., Goeken, R.M., Goldstein, S., Hirsch, V.M., Martin, M.A., 2004. Highly pathogenic SHIVs and SIVs target different $CD4^+$ T cell subsets in rhesus monkeys, explaining their divergent clinical courses. Proc. Natl. Acad. Sci. U. S. A. 101, 12324–12329.

O'Brien, W.A., Hartigan, P.M., Martin, D., Esinhart, J., Hill, A., Benoit, S., Rubin, M., Simberkoff, M.S., Hamilton, J.D., 1996. Changes in plasma HIV-1 RNA and $CD4^+$ lymphocyte counts and the risk of progression to AIDS. Veterans Affairs Cooperative Study Group on AIDS. N. Engl. J. Med. 334, 426–431.

Okoye, A., Meier-Schellersheim, M., Brenchley, J.M., Hagen, S.I., Walker, J.M., Rohankhedkar, M., Lum, R., Edgar, J.B., Planer, S.L., Legasse, A., Sylwester, A.W., Piatak Jr., M., Lifson, J.D., Maino, V.C., Sodora, D.L., Douek, D.C., Axthelm, M.K., Grossman, Z., Picker, L.J., 2007. Progressive $CD4^+$ central memory T cell decline results in $CD4^+$ effector memory insufficiency and overt disease in chronic SIV infection. J. Exp. Med. 204, 2171–2185.

Okuma, K., Tanaka, R., Ogura, T., Ito, M., Kumakura, S., Yanaka, M., Nishizawa, M., Sugiura, W., Yamamoto, N., Tanaka, Y., 2008. Interleukin-4-transgenic hu-PBL-SCID mice: a model for the screening of antiviral drugs and immunotherapeutic agents against X4 HIV-1 viruses. J. Infect. Dis. 197, 134–141.

Pedroza-Martins, L., Gurney, K.B., Torbett, B.E., Uittenbogaart, C.H., 1998. Differential tropism and replication kinetics of human immunodeficiency virus type 1 isolates in thymocytes: coreceptor expression allows viral entry, but productive infection of distinct subsets is determined at the postentry level. J. Virol. 72, 9441–9452.

Roeth, J.F., Collins, K.L., 2006. Human immunodeficiency virus type 1 Nef: adapting to intracellular trafficking pathways. Microbiol. Mol. Biol. Rev. 70, 548–563.

Sallusto, F., Geginat, J., Lanzavecchia, A., 2004. Central memory and effector memory T cell subsets: function, generation, and maintenance. Annu. Rev. Immunol. 22, 745–763.

Sato, K., Aoki, J., Misawa, N., Daikoku, E., Sano, K., Tanaka, Y., Koyanagi, Y., 2008. Modulation of human immunodeficiency virus type 1 infectivity through incorporation of tetraspanin proteins. J. Virol. 82, 1021–1033.

Schnittman, S.M., Denning, S.M., Greenhouse, J.J., Justement, J.S., Baseler, M., Kurtzberg, J., Haynes, B.F., Fauci, A.S., 1990. Evidence for susceptibility of intrathymic T-cell precursors and their progeny carrying T-cell antigen receptor phenotypes $TCR\alpha\beta^+$ and $TCR\gamma\delta^+$ to human immunodeficiency virus infection: a mechanism for $CD4^+$ (T4) lymphocyte depletion. Proc. Natl. Acad. Sci. U. S. A. 87, 7727–7731.

Sereti, I., Sklar, P., Ramchandani, M.S., Read, S.W., Aggarwal, V., Imamichi, H., Natarajan, V., Metcalf, J.A., Kovacs, J.A., Tavel, J., Davey, R.T., Dersimonian, R., Lane, H.C., 2007. $CD4^+$ T cell responses to interleukin-2 administration in HIV-infected patients are

directly related to the baseline level of immune activation. J. Infect Dis. 196, 677–683.
Stevenson, M., Stanwick, T.L., Dempsey, M.P., Lamonica, C.A., 1990. HIV-1 replication is controlled at the level of T cell activation and proviral integration. EMBO J. 9, 1551–1560.
Traggiai, E., Chicha, L., Mazzucchelli, L., Bronz, L., Piffaretti, J.C., Lanzavecchia, A., Manz, M.G., 2004. Development of a human adaptive immune system in cord blood cell-transplanted mice. Science 304, 104–107.
Vatakis, D.N., Bristol, G., Wilkinson, T.A., Chow, S.A., Zack, J.A., 2007. Immediate activation fails to rescue efficient human immunodeficiency virus replication in quiescent CD4$^+$ T cells. J. Virol. 81, 3574–3582.
Wilpshaar, J., Falkenburg, J.H., Tong, X., Noort, W.A., Breese, R., Heilman, D., Kanhai, H., Orschell-Traycoff, C.M., Srour, E.F., 2000. Similar repopulating capacity of mitotically active and resting umbilical cord blood CD34$^+$ cells in NOD/SCID mice. Blood 96, 2100–2107.
Ye, P., Kirschner, D.E., Kourtis, A.P., 2004. The thymus during HIV disease: role in pathogenesis and in immune recovery. Curr. HIV Res. 2, 177–183.
Zack, J.A., Arrigo, S.J., Weitsman, S.R., Go, A.S., Haislip, A., Chen, I.S., 1990. HIV-1 entry into quiescent primary lymphocytes: molecular analysis reveals a labile, latent viral structure. Cell 61, 213–222.
Zhang, Z., Schuler, T., Zupancic, M., Wietgrefe, S., Staskus, K.A., Reimann, K.A., Reinhart, T.A., Rogan, M., Cavert, W., Miller, C.J., Veazey, R.S., Notermans, D., Little, S., Danner, S.A., Richman, D.D., Havlir, D., Wong, J., Jordan, H.L., Schacker, T.W., Racz, P., Tenner-Racz, K., Letvin, N.L., Wolinsky, S., Haase, A.T., 1999. Sexual transmission and propagation of SIV and HIV in resting and activated CD4$^+$ T cells. Science 286, 1353–1357.
Zhang, Z.Q., Wietgrefe, S.W., Li, Q., Shore, M.D., Duan, L., Reilly, C., Lifson, J.D., Haase, A.T., 2004. Roles of substrate availability and infection of resting and activated CD4$^+$ T cells in transmission and acute simian immunodeficiency virus infection. Proc. Natl. Acad. Sci. U. S. A. 101, 5640–5645.

ELSEVIER

Experimental Hematology

Experimental Hematology 2009;37:1400–1410

Bone marrow engraftment but limited expansion of hematopoietic cells from multipotent germline stem cells derived from neonatal mouse testis

Momoko Yoshimoto[a,b], Toshio Heike[a], Hsi Chang[a], Mito Kanatsu-Shinohara[c], Shiro Baba[a], Joseph T. Varnau[b], Takashi Shinohara[c], Mervin C. Yoder[b], and Tatsutoshi Nakahata[a]

[a]*Departments of Pediatrics, Kyoto University, Kyoto, Japan;*
[b]*Department of Pediatrics, Herman B Wells Center for Pediatric Research, Indiana University School of Medicine, Indianapolis, Ind., USA;*
[c]*Molecular Genetics, Graduate School of Medicine, Kyoto University, Kyoto, Japan*

(Received 28 March 2009; revised 1 September 2009; accepted 21 September 2009)

Objective. **Multipotent germline stem (mGS) cells derived from neonatal mouse testis, similar to embryonic stem (ES) cells, differentiate into various types of somatic cells in vitro and produce teratomas after inoculation into mice. In the present work, we examined mGS cells for hematopoietic progenitor potential in vitro and in vivo.**

Materials and Methods. **mGS cells were differentiated on OP9 stromal cells and induced into Flk1$^+$ cells. Flk1$^+$ cells were sorted and replated on OP9 stromal cells with various cytokines and emerging hematopoietic cells were analyzed for lineage marker expression by fluorescein-activated cell sorting, progenitor activity by colony assay, and stem cell transplantation assay.**

Results. **mGS cells, like ES cells, produce hematopoietic progenitors, including both primitive and definitive erythromyeloid, megakaryocyte, and B- and T-cell lineages via Flk1$^+$ progenitors. When transplanted into the bone marrow (BM) of nonobese diabetic/severe combined immunodeficient (NOD/SCID) γc^{null} mice directly, mGS-derived green fluorescent protein (GFP)-positive cells were detected 4 months later in the BM and spleen. GFP$^+$ donor cells were also identified in the Hoechst33342 side population, a feature of hematopoietic stem cells. However, these mGS-derived hematopoietic cells did not proliferate in vivo, even after exposure to hematopoietic stressors, such as 5-fluorouracil (5FU) injection or serial transplantation.**

Conclusion. **mGS cells produced multipotent hematopoietic progenitor cells with myeloid and lymphoid lineage potential in vitro and localized in the BM after intra-BM injection but, like ES cells, failed to expand or show stem cell repopulating ability in vivo.** © **2009 ISEH - Society for Hematology and Stem Cells. Published by Elsevier Inc.**

Hematopoietic stem cells (HSCs) are defined as blood cells displaying the potential for self-renewal and multilineage differentiation. HSC transplantation has been widely used for treating hematological malignancies and inherited disorders. Peripheral blood and cord blood stem cells, as well as bone marrow cells, have been intensively studied and shown to be effective for clinical use. Recently, embryonic stem (ES) cells have been proposed as an alternative candidate source of HSCs. Many approaches have been attempted to obtain HSCs from ES cells, but this is challenging unless using enforced expression of genes, such as *Hoxb4* [1] or *Cdx4* [2] in ES cells. Even if a robust method for HSC derivation from ES cells were discovered, one would still need to address donor–host differences in histocompatibility antigens to permit ES-derived HSC engraftment in patients.

Multipotent germline stem (mGS) cells have been established from neonatal mouse testis and have been proven to have similar potential to ES cells, including germline transmission [3]. If mGS cells could be isolated from human testis and were utilized to produce HSC, then the problem of major histocompatibility complex (MHC) incompatibility would be solved because it might be possible to establish the patient's own mGS cells. In that sense, mGS cells may have a big advantage over ES cells in human application for cell therapies.

The methods for inducing hematopoietic cells from ES cells have been well-developed [4]. Flk1 is a candidate marker for mesoderm [5] and hemangioblast [6,7] cells, and Flk1 progeny have been proven to differentiate into

Offprint requests to: Momoko Yoshimoto, M.D., Ph.D., Wells Center for Pediatric Research, Indiana University School of Medicine, Indianapolis, IN 46202, USA; E-mail: myoshimo@iupui.edu

0301-472X/09 $–see front matter.
doi: 10.1016/j.exphem.2009.09.006

all hematopoietic cell lineages [8]. Using the OP9 stromal cell line as a feeder layer, hematopoietic cells are effectively induced from ES cells [9], and $FLK1^+$-derived definitive hematopoietic cells are obtained [10].

In a previous report [3], mGS cells have been shown to differentiate into $CD45^+$ hematopoietic cells, including $Gr\text{-}1^+Mac1^+$ myeloid cells and $Ter119^+$ erythroid cells, but the potential for mGS cells to differentiate into hematopoietic stem/progenitor has not been reported. We have observed multipotent hematopoietic progenitor cells with myeloid and lymphoid potential emerging from mGS $FLK1^+$ cells using the OP9 feeder cell system and describe the localization of mGS-derived hematopoietic cells in the bone marrow (BM) cavity when directly injected into the BM of immunodeficient mice. However, the mGS-derived hematopoietic cells present in the host, like differentiated wild-type ES-derived hematopoietic cells, do not proliferate or display multilineage repopulating ability in vivo.

Materials and methods

Cell culture

mGS cells were established from mouse neonatal testis of DBA/2 mice or a green fluorescent protein (GFP)–expressing transgenic mouse (C57BL6 x DBA/2 F1 background), as described previously [3]. The CCE ES cell line was kindly provided by Dr. S. Nishikawa (RIKEN, Kobe, Japan). The ES cell line D3 was transfected with GFP gene driven by the ubiquitous CAG promoter. These CCE and D3 cell lines are derived from the 129 mouse strain. GFP^+ mGS and D3 were used for the transplantation assay. The mGS or ES lines were maintained as described previously [3].

Differentiation to hematopoietic progenitor cells was induced as described [8,11]. Briefly, 10^4 of undifferentiated mGS and ES cells were seeded onto T-25 flask with confluent OP9 stromal cells (a gift from Dr. Kodama) in α–minimum essential medium supplemented with 10% fetal bovine serum and 5×10^{-5}M 2-mercaptoenthanol. After 4 days, cultured cells were harvested with cell dissociation buffer (Gibco, Grand Island, NY, USA) and $Flk1^+$ cells were collected using a FACSVantage flow cytometer (Becton Dickinson, Mountain View, CA, USA). The $5\text{–}10 \times 10^3$ $Flk1^+$ cells per well in six-well plate with confluent OP9 stromal cells were cocultured again with added cytokines, such as 100 ng/mL mouse stem cell factor (SCF), 10 ng/mL human thrombopoietin (TPO), 10 ng/mL mouse Flt-3 ligand (FL), 4 u/mL human erythropoietin (EPO), and 100 u/mL mouse interleukin (IL)-7. Mouse SCF, human TPO, and human EPO were kindly provided from Kirin Brewery (Tokyo, Japan). Mouse FL and IL-7 were purchased from R&D Systems (Minneapolis, MN, USA). For T-cell induction, $Flk1^+$ cells were cocultured with OP9-DL1 [12] stromal cells (kindly provided by Dr. Zuniga-Pflucker, University of Toronto) with 50 ng/mL IL-7.

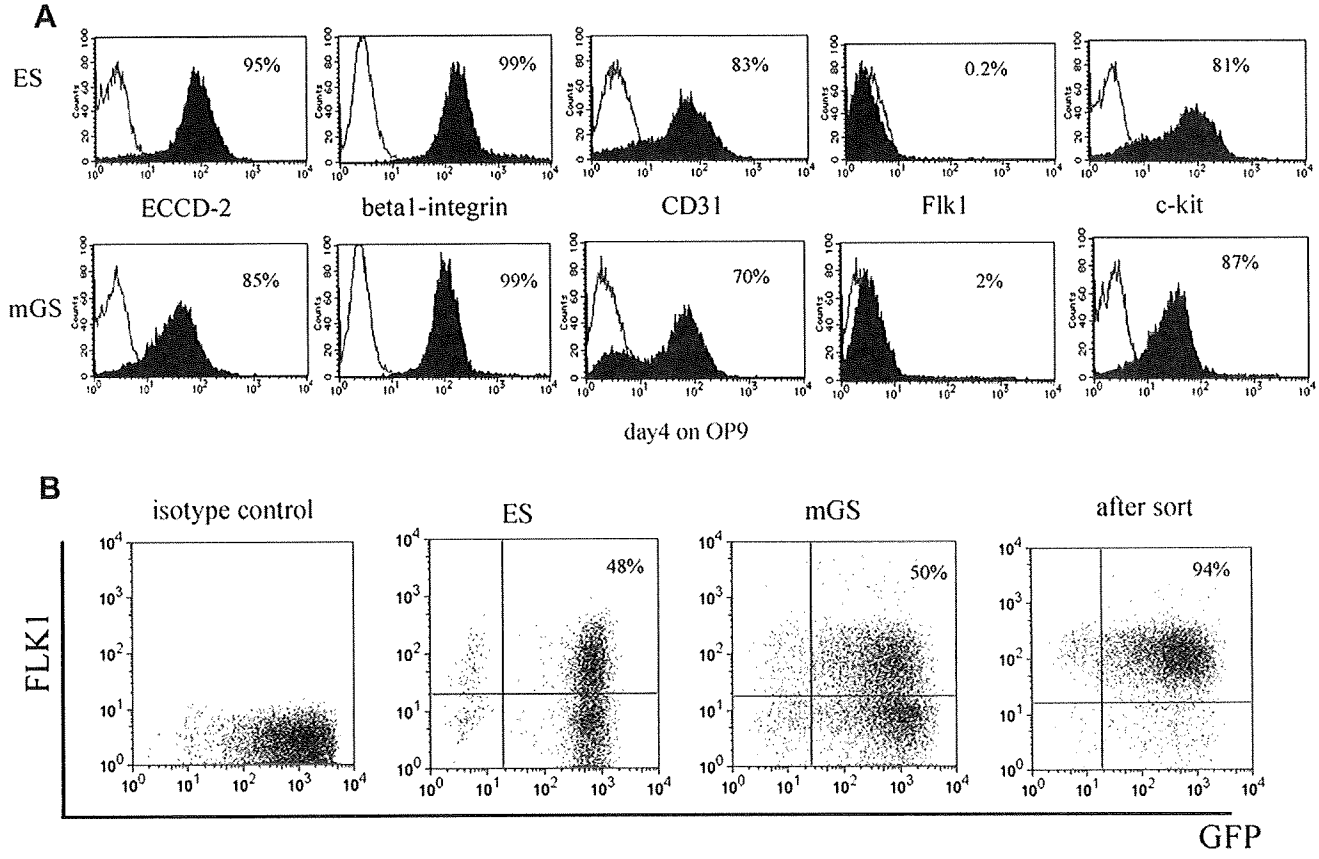

Figure 1. Surface markers of mGS and ES cells. Surface markers of undifferentiated mGS cells (**A**, lower panel) are similar to those of ES cells (**A**, upper panel). mGS cells were induced on OP9 stromal cells for 4 days and were confirmed to express Flk1 (**B**).

Hematopoietic colony-forming cell assay

In order to analyze emergence of immature hematopoietic progenitor cells from mGS cells, on each day after induction of Flk1$^+$ cells on OP9, cells were harvested and plated in methylcellulose for colony-forming assay using a modification of the technique described previously [13,14]. All cultures were performed in triplicate and the number of colony-forming cells was scored at day 8 to 10. For megakaryocyte colonies, the cells were plated in Megacult (Stem Cell Technologies, Vancouver, Canada) according to manufacturer's instruction.

Antibodies and staining

The following primary antibodies were used: rat anti-mouse E-cadherin (ECCD2, from Calbiochem. San Diego, CA, USA), fluorescein isothiocyanate (FITC)–conjugated hamster anti-rat β1 integrin (Ha2/5), rat anti-mouse CD31 (MEC 13.3), allophycocyanin (APC)-conjugated rat anti-mouse *c-kit* (2B8), phycoerythrin (PE)-conjugated rat anti-Flk1 (AVAS12), PE-conjugated rat anti-mouse Ter119 (TER-119), APC-conjugated rat anti-mouse CD45 (30-F11), biotin-conjugated rat anti-mouse Gr-1 (RB6-8C5), biotin-conjugated rat anti-mouse Mac-1 (M1/70), purified rat CD41 antibody (MWReg30), and rabbit anti-embryonic hemoglobin antibody [15] (a gift from Dr. Takakura, Osaka University). PE-conjugated or alkaline phosphatase–conjugated anti-rat IgG, APC-conjugated streptavidin, or FITC–conjugated anti-rabbit immunoglobulin G were used as secondary antibodies. All antibodies except ECCD2 were purchased from Pharmingen (San Diego, CA, USA). For detection of side population (SP) cells, BM cells were stained with Hoechst 33324, as described previously [16–18]. Stained cells were analyzed using FACSCalibur or LSRII (Becton Dickinson).

Immunohistochemistry

Femurs of recipient mice were fixed with 4% paraformaldehyde, embedded in the optimal cutting temperature compound and frozen sections of 7-μm thickness were mounted on silan-coated glass slides and were stained with rabbit anti-GFP antibody (BD Bioscience Clontech, Palo Alto, CA, USA), as described previously [19]. Cytospin preparations and culture dishes were also stained with various antibodies, as described previously [20,21].

Mice and transplantation

Nonobese diabetic/severe combined immunodeficient (NOD/SCID) γc^{null} mice were kindly provided from the Central Institute of Experimental Animals (Kawasaki, Japan) and kept under specific pathogen-free conditions in accordance with the guidelines of the facility. Cultured mGS-derived hematopoietic cells and OP9 cells were collected and injected into the femoral BM of NOD/SCIDγc^{null} mice that were irradiated with 2.4 Gy before transplantation. The 2×10^5 BM mononuclear cells were injected as a positive control. After transplantation, mice were prophylactically provided sterile water with neomycin sulfate (Gibco BRL).

For serial transplantation, BM cells were collected from transplanted NOD/SCIDγc^{null} mice 4 months after primary transplantation and stained with anti-CD45.1$^+$ (recipient) and CD45.2$^+$ (donor) antibodies. CD45.2$^+$ donor cells were sorted on FACSVantage (Becton Dickinson) and injected into the BM of 2.4-Gy irradiated NOD/SCIDγc^{null} mice. Peripheral blood (PB) and BM were analyzed 3 to 4 months after secondary transplantation.

RNA extraction and reverse transcriptase polymerase chain reaction (RT-PCR) analysis

Total RNA was prepared using Trisol (Gibco BRL). Complementary DNA (cDNA) synthesis was performed using Superscript II

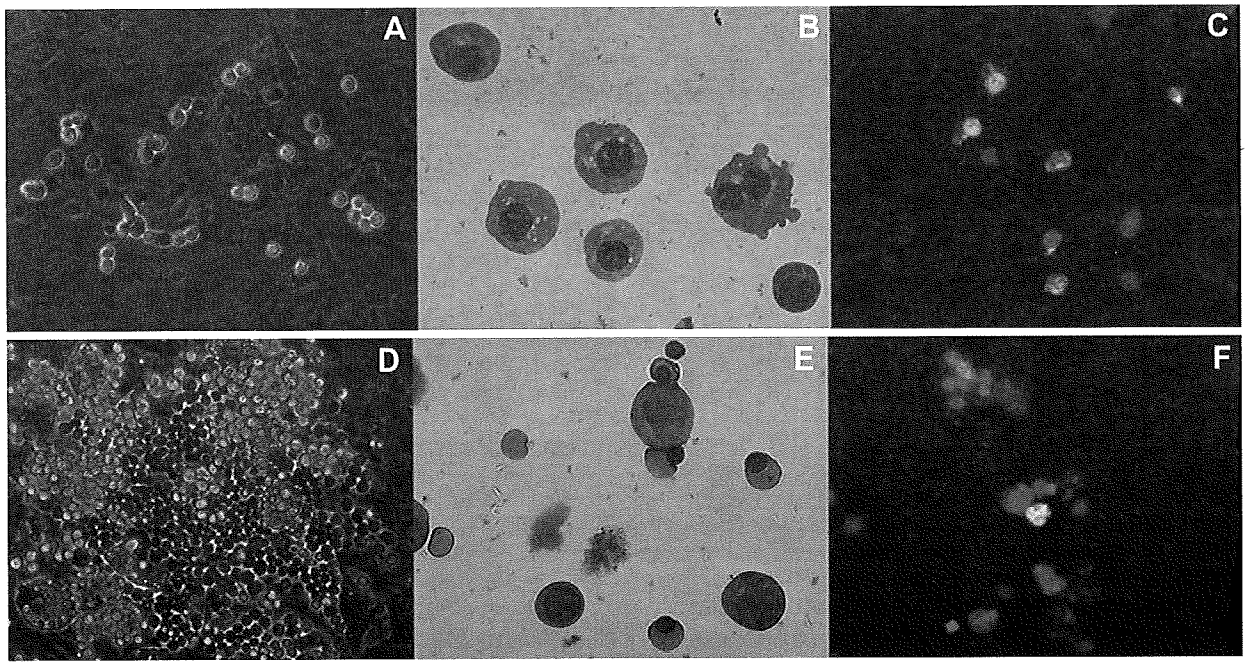

Figure 2. Primitive and definitive erythroid cells are differentiated from mGS–derived Flk1$^+$ cells. mGS-derived Flk1$^+$ cells were cultured on OP9 cells and small round cells and cobblestone-forming areas were found [(**A**) day 3, (**D**) day 9). May-Giemsa staining of a cytospin preparation [(**B**); day 3, (**E**); day 9)]. Immunostaining of E1 antigen and Ter119 (**C**,**F**). (**C**) E1 antigen; green. (**F**) E1 antigen; green Ter119; red. Nuclear staining with Hoechst 33324; blue. Magnification (**A**,**D**): ×100; (**B**,**C**,**E**,**F**): ×200.

and oligo $(dT)_{12-18}$ primers (Invitrogen, Carlsbad, CA, USA) following manufacturer's instructions. The same cDNA sample was used for PCR amplification with different primer sets, using standard protocols using AmpliTaq Gold (Applied Biosystems, Foster City, CA, USA). The primer sequences were as follows: βH1 forward: AGTCCCCATGGAGTCAAAGA, reverse: CTC AAG GAG ACC TTT GCT CA, β major forward: CTG ACA GAT GCT CTC TTG GG, reverse: CAC AAA CCC CAG AAA CAG ACA, GAPDH forward: TCC CAC TCT TCC ACC TTC, reverse: CTG TAG CCG TAT TCA TTG TC. For PCR to detect GFP, the primer sequence were as follows: GFP forward: CTG GTC GAG CTG GAC GGC GAC G, reverse: CAC GAA CTC CAG CAG GAC CAT G. Cycling parameters included: denaturation at 94°C for 30 seconds; annealing at various temperatures for 30 seconds; elongation at 72°C for 40 seconds. The number of cycle varied between 25 and 35 cycles.

Results

mGS cells can differentiate into Flk1$^+$ cells on OP9 stromal cells

It has been reported that mGS cells are very similar to ES cells in their differentiation ability into multiple cell lineages in vitro and in vivo [3]. Undifferentiated mGS and ES cells express ECCD-2, β1-integrin, CD31 and c-kit, but are negative for Flk-1 expression (Fig. 1A). In order to examine the differentiation potential of these cells, we cocultured mGS or ES cells with OP9 stromal cells and assayed for emergence of Flk1$^+$ cells 4 days after induction because Flk1 is thought to be a representative marker for mesodermal cells [5]. The percentage of Flk1$^+$ cells derived from mGS cells (50%) was very similar to ES cells (48%) (Fig. 1B).

Primitive and definitive erythropoiesis can be derived in vitro in mGS culture

In order to examine red blood cell emergence from mGS-derived Flk1$^+$ cells, Flk1$^+$ cells were sorted and cocultured on OP9 stromal cells with added EPO. Three days later, small round hematopoietic cells were found (Fig. 2A). The cytospin preparation of these cells and May-Giemsa staining revealed the round, nucleated cell morphology of primitive erythrocytes (Fig. 2B). Immunostaining with an antiembryonic hemoglobin antibody confirmed that these cells were primitive erythrocytes (Fig. 2C). After 9 days of coculture, cobblestone-forming areas were observed in

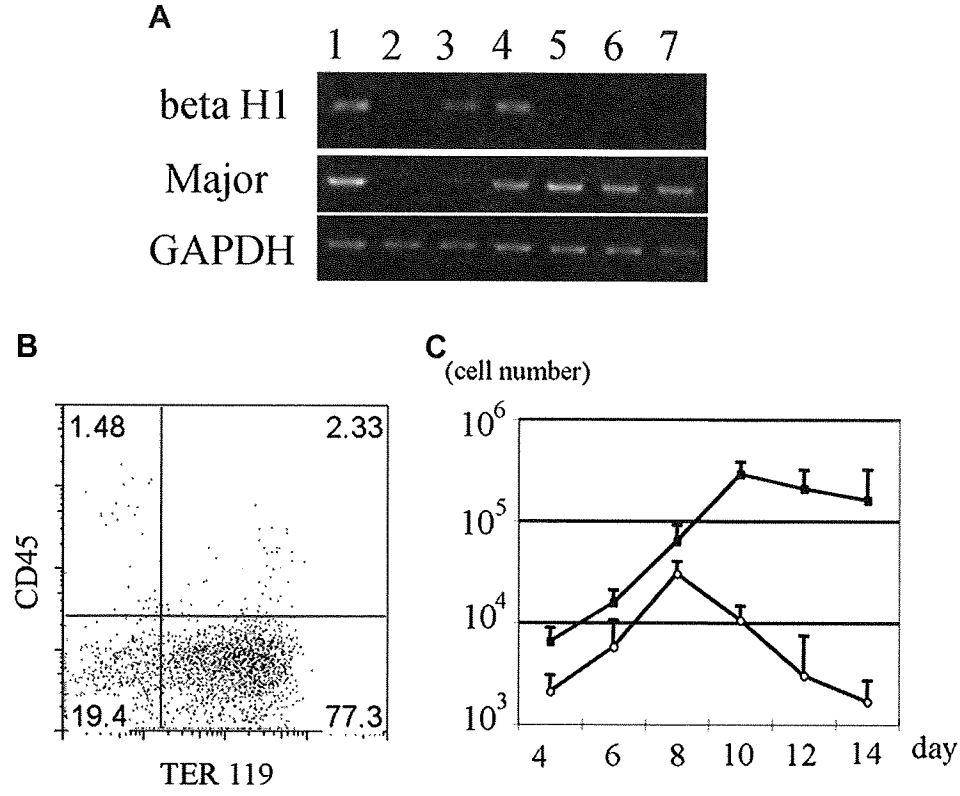

Figure 3. Erythropoiesis from mGS Flk1$^+$ cells shows two different waves. Flk1$^+$ cells were cultured on OP9 with erythropoietin (EPO) and with or without ACK45. The nonadherent cells in the culture were collected every other day, counted the number (**C**), examined the surface markers (**B**) and hemoglobin gene expression (**A**). Sequential RT-PCR analysis shows expression of β H1 hemoglobin mRNA, followed by β-major hemoglobin mRNA expression (**A**). E12.5 fetal liver (lane 1), E8.0 embryo (lane 2), mGS- Flk1$^+$ cells on OP9 for 4 days (lane 3), for 6 days (lane 4), for 8 days (lane 5), for 10 days (lane 6), for 12 days (lane 7). Flk1$^+$ cells were cultured on OP9 cells with EPO and with (white circle) or without ACK45 (black square) (**C**). Most cells in the culture were Ter119$^+$ erythrocyte (**B**). Definitive erythropoiesis was blocked by ACK45 (**C**). GAPDH = glyceraldehydes phosphate dehydrogenase.

the cultures (Fig. 2D). Morphologic analysis of nonadherent cells revealed enucleated red blood cells (Fig. 2E). Immunostaining confirmed the cells to be definitive erythrocytes that express Ter119, but not embryonic hemoglobin molecules (Fig. 2F). Next, mGS Flk1$^+$ cells were cocultured on OP9 cells in the presence of EPO or EPO and Ack45 (a blocking antibody of the c-kit signaling pathway). In this culture system, most of the emerging blood cells were Ter119$^+$ erythroid cells (Fig. 3B), but the growth factor requirements of the cultured cells in each condition showed different patterns: an initial c-kit–independent period (days 4–8; Fig. 3C) and a second c-kit–dependent period during which erythropoiesis was blocked by the presence of the Ack45 antibody (days 8–14, Fig. 3C). Erythrocytes in the initial wave expressed βH1 hemoglobin mRNA, while only β-major hemoglobin mRNA was expressed in the second wave of erythropoiesis (Fig. 3A). These results indicated that cells in the initial wave represented primitive erythrocytes, while definitive erythrocytes comprised the second wave [22]. Thus, mGS cells can give rise to primitive and definitive erythropoiesis in vitro in the same manner as differentiated ES cells.

Flk1$^+$ cells derived from mGS cell can differentiate into multiple lineages including B and T cells

When mGS-derived Flk1$^+$ cells were cocultured on OP9 cells with added SCF, granulocyte colony-stimulating factor (G-CSF), IL-3, and EPO, Flk1$^+$ cells can also differentiate into Mac1$^+$Gr1$^+$ cells and Ter119$^+$ cells (7.3% and 20.9%, respectively) similar to ES cells (7.6% and 24.3%, respectively) (Fig. 4A). Furthermore, mGS-derived Flk1$^+$ cells also gave rise to CD19$^+$ B cells and CD4$^+$CD8$^+$ T cells when cultured on OP9 cells or OP9-DL1 cells with added IL7 (Fig. 4C and D).

Flk1$^+$ cells derived from mGS cell can differentiate into multipotent progenitors

To determine whether mGS cells can give rise to clonogenic hematopoietic progenitors, Flk1$^+$ cells derived from mGS cells were cocultured on OP9 cells and all the cells after 4 to 10 days culture were plated in methylcellulose with added growth factors. Burst-forming unit-erythroid (BFU-E), colony-forming unit granulocyte-macrophage (CFU-GM), and CFU-Mix were observed (Fig. 5Aa–d). Interestingly, the number of CFU-mix was decreased after 8 days' coculture (Fig. 5Ba), and CFU-GM was the main

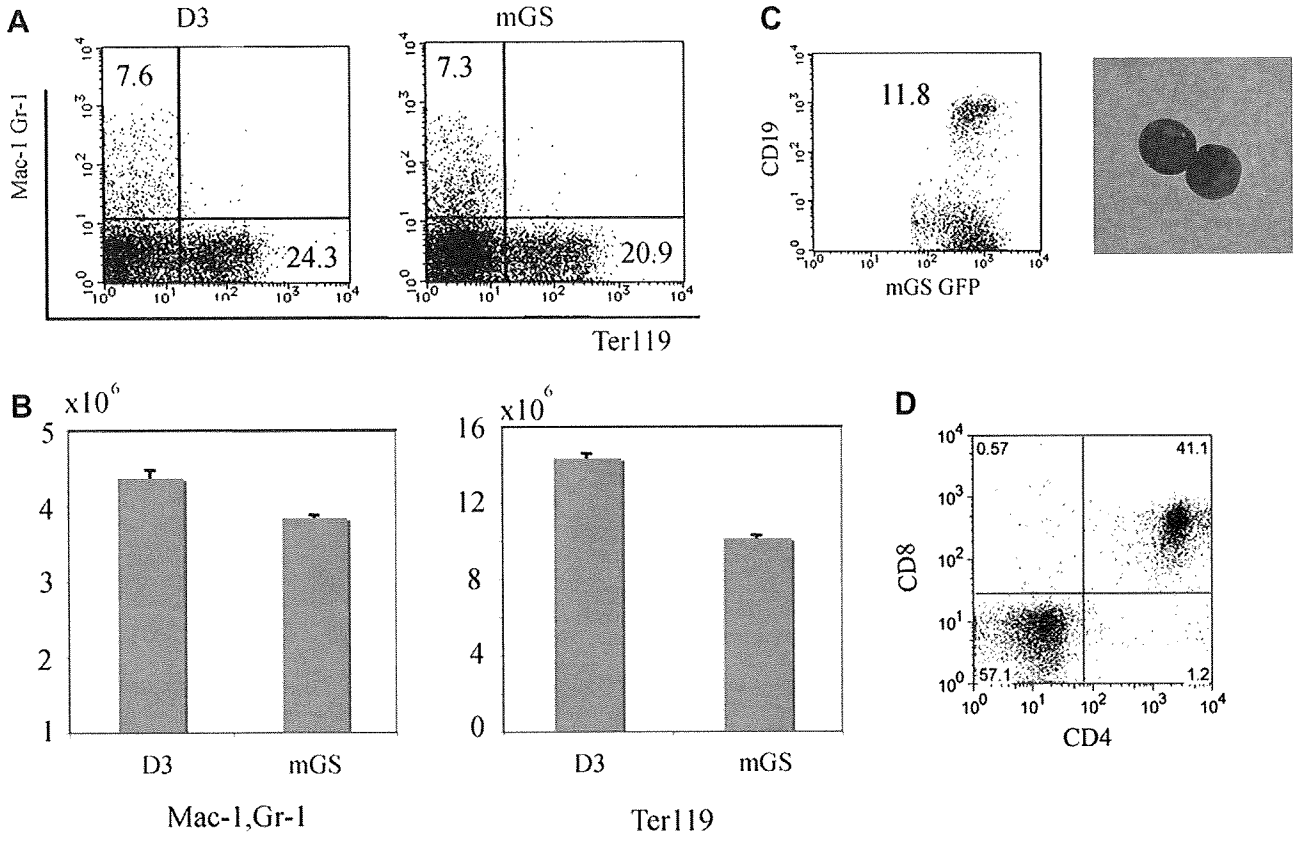

Figure 4. Myelolymphoid potential of mGS cells. Mac1$^+$Gr1$^+$, Ter119$^+$, CD19$^+$, and CD4$^+$CD8$^+$ cells were differentiated from mGS-derived Flk-1$^+$ cells within OP9 culture (**A**,**B**,**C**) or OP9-DL1 culture (**D**). For Mac1$^+$Gr1$^+$, Ter119$^+$ cells, cells were collected from 8–10 days culture (**A**,**B**). The numbers of myeloid and erythroid cells differentiated from mGS and ES cells were similar (**B**). For CD19$^+$ (**C**), and CD4$^+$CD8$^+$ cells (**D**), cells were collected from 14–21 days culture. These FACS data are representative among three independent experiments.

population detectable after 10 day's culture of mGS cells on OP9 cells. To examine whether production of these clonogenic progenitors from Flk1$^+$ cells was influenced by cytokines, Flk1$^+$ cells were cocultured on OP9 cells with only EPO or with SCF, TPO, and FL. The numbers of all kind of colonies were increased when cocultured with SCF, TPO, and FL (Fig. 5Bb). Thus, mGS-derived Flk1$^+$ cells generate multipotent hematopoietic progenitors, and this effect was promoted by addition of multiple cytokines, similar to differentiated ES cells.

Megakaryopoiesis through Flk1$^+$ cells derived from mGS cells

We also evaluated megakaryocyte production from mGS-derived Flk1$^+$ cells. Eight days after Flk1$^+$ cells were cocultured on OP9 cells in the presence of TPO and SCF, large round cells with proplatelets were observed (Fig. 5Ca). These cells expressed the cell surface protein CD41, a well-recognized marker of the platelet lineage (Fig. 5Cb). Cytospin preparations of culture fluid from these culture dishes showed large multinucleated cells that were CD41-positive (Fig. 5Cc and Cd). These cells contained both CFU-megakaryocyte and CFU-mega-mix confirmed by specific megakaryocyte progenitor cultures (Fig. 5Ce and Cf). CFU-megakaryocyte progenitors were maintained during culturing between day 8 and day 12 of mGS-derived Flk1$^+$ cells in the presence of TPO and SCF (Fig. 5D). Differentiated ES cells also showed similar trends of megakaryocyte colony production (data not shown). Thus, Flk1$^+$ cells derived from mGS cells were shown to produce megakaryocytes as well as megakaryocyte progenitor cells.

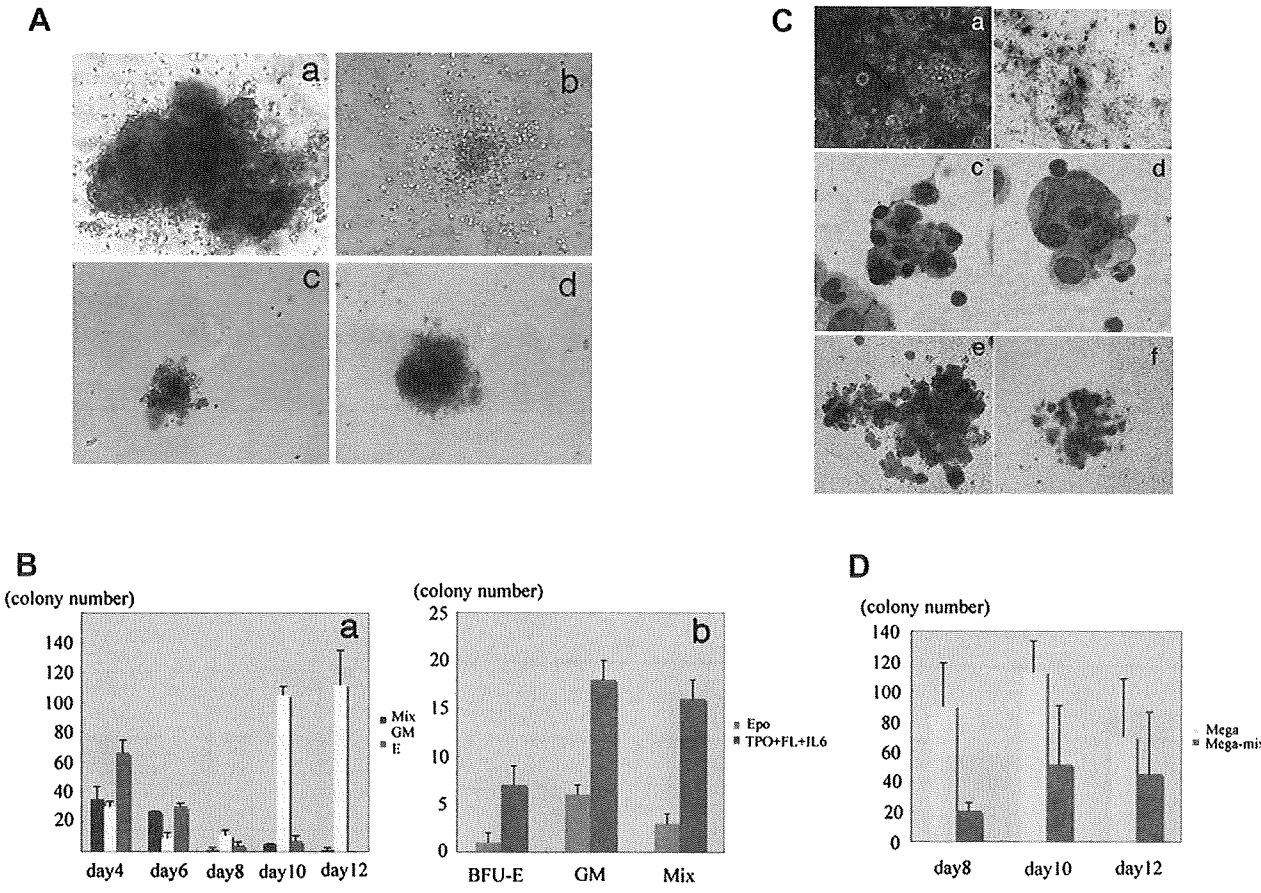

Figure 5. Colony-forming ability and megakaryocyte potential of mGS Flk1$^+$-derived cells. mGS-derived Flk-1$^+$ cells produce hematopoietic progenitor cells that can form various kinds of colonies [(**Aa**) mixed colony, (**Ab**) granulocyte-macrophage (GM) colony, (**Ac**) burst-forming unit erythroid (BFU-E), (**Ad**) mast cell colony]. Mixed colonies were predominant when mGS-derived Flk1$^+$ cells were cultured on OP9 cells for 4 to 6 days (**Ba**). Blue bar: mixed colony, yellow bar: GM colony, red bar: Erythroid colony. The number of all kinds of colonies was increased when mGS Flk1$^+$ cells were cultured on OP9 with thrombopoietin (TPO) and interleukin (IL)-6 (**Bb**). Blue bar: with erythropoietin (EPO), red bar: with TPO and IL6. Megakaryocyte or proplatelet mGS-derived Flk1$^+$ cells were observed within OP9 culture for 8–12 days. Proplatelet like cells (arrow **Ca**), Immunostaining of cultured cells with CD41 antibody secondary detected by alkaline phosphatase–conjugated antibody (**Cb** blue). Immunostaining of a cytospin preparation with CD41 antibody secondary detected by peroxidase conjugated antibody (**Cc**, **Cd** brown). After transferring cultured cells into Megacult conditions, megakaryocyte colonies (**Cf**) include mega-mix colonies (**Ce**) were found. These cells expressed acethylcholinestrase as evidenced by brown staining. The CFU-Mega was maintained during culturing day 8 to 12 in the presence of TPO and stem cell factor (**D**). Yellow bar: Megakaryo-colony, red bar: Mega-Mix colony. Magnification: (**Ca, Cb**) ×100; (**Cc**, **Cd**) ×200; (**Ce**, **Cf**) ×100.

Flk1-derived hematopoietic cells can engraft in the BM of NOD/SCIDγc^{null} mice by intra-BM injection

Finally, day-6 cocultured mGS-derived Flk1$^+$ cells and OP9 cells were recovered and injected directly into the BM of NOD/SCIDγc^{null} mice (n = 4). As a positive control, 2 × 10^5 BM mononuclear cells were injected into the BM of NOD/SCIDγc^{null} mice. Every 4 weeks after transplantation, PB was analyzed for evidence of donor-cell engraftment. While the BM cells engrafted, mGS-derived cells were barely detected (<0.1%, Fig. 6A). After 7 weeks, fluorescein-activated cell sorting (FACS) analysis revealed donor mGS-derived GFP$^+$ cells in the BM, but at low chimerism of <0.1% (data not shown). PCR analysis confirmed the presence of GFP-DNA in the BM and the spleen (Fig. 6C). Four months after transplantation, a very small number of donor CD45$^+$GFP$^+$ cells were detected in the BM and the spleen by FACS analysis and confirmed by PCR (Fig. 6A, C, and D). Furthermore, when BM cells of transplanted mice were stained with Hoechst33324, GFP$^+$ cells were detected in the SP region (Fig. 6E and F). Immunostaining of the femur revealed that GFP$^+$ cells were attached to the endosteal region, where HSCs are considered to reside (Fig. 6B). Three of four transplanted mice were confirmed to display this type of "stem cell-like" engraftment (0.03% ± 0.03%). Thus, mGS-derived hematopoietic cells are found in the BM 4 months after transplantation. It is of note that no teratoma formation was observed in any of the transplanted animals.

mGS-derived hematopoietic cells did not show stem cell potential by serial transplantation

Because HSCs are enriched in the SP fraction and normally reside in the endosteal region of the BM [23–25], we speculated that hematopoietic progeny of mGS-derived Flk1$^+$ cells engrafted in the BM and remained in the stem cell fraction. In order to prove that these GFP$^+$ cells in the BM were HSCs, we hypothesized that hematopoietic stress may induce further expansion of the donor HSCs and thus, 5FU injection and serial transplantation were performed. 5FU was injected intraperitoneally at a standard dose of 100 ug/g into transplanted mice that received mGS-derived hematopoietic cells and the PB was analyzed with CD45.1 and CD45.2 antibodies every week after 5FU injection. When the blood cell count recovered, we expected donor-derived cells would increase in number in PB, however, no donor mGS-derived cells were observed (data not shown). For secondary transplantation analysis, we

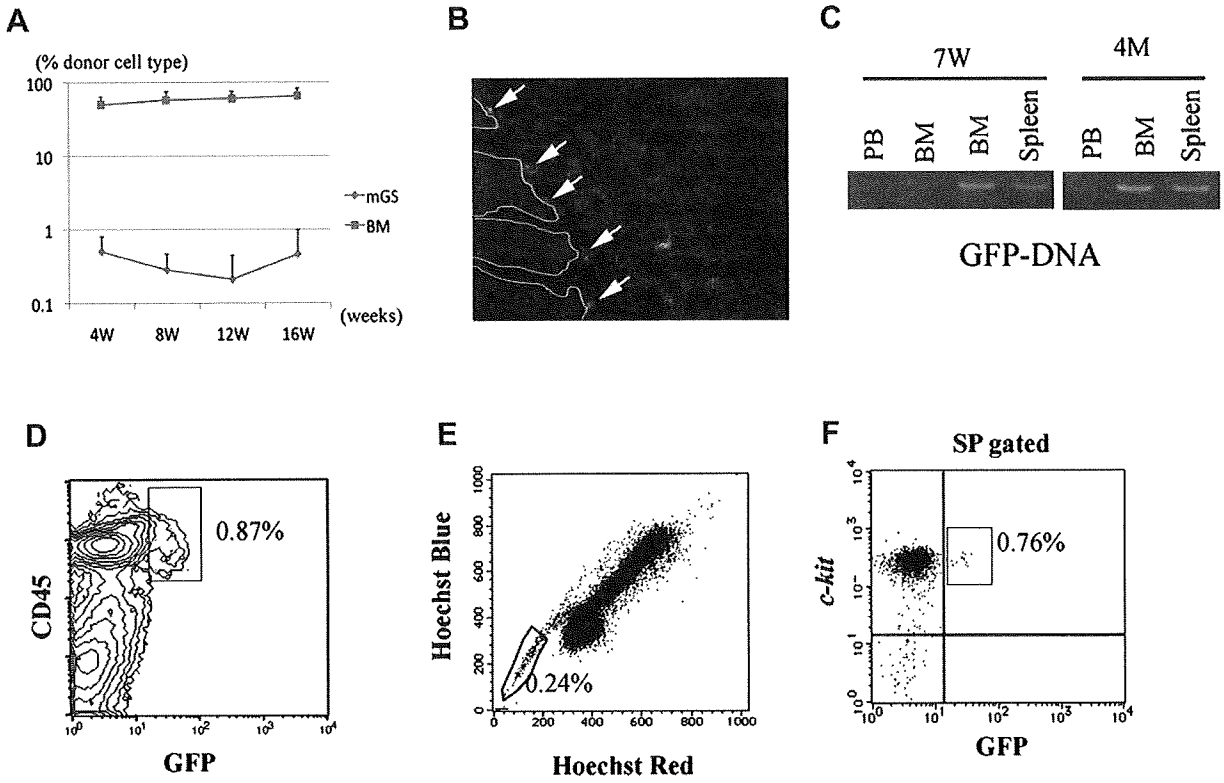

Figure 6. Transplanted hematopoietic cells from GFP$^+$ mGS cells can be detected in bone marrow (BM) 4 months after transplantation and displays stem cell phenotype. After transplantation, peripheral blood (PB) was analyzed every 4 weeks (**A**). BM cells from recipient mice 4 months after transplantation were analyzed by LSR II (**D**, **E**, **F**). GFP$^+$CD45$^+$ cells were detected (**D**). When the BM cells of the recipient mice were stained with Hoechst 33324, GFP$^+$ cells were detected in the SP region (**E**, **F**). In the section of recipient BM, GFP$^+$ cells were found attached to the endosteal region (**B**, arrow). RT-PCR shows donor-derived DNA in the BM and spleen at 7 weeks and 4 months after transplantation (**C**).

collected BM cells of primary recipient mice. Interestingly, more donor cells were detected in the lineage-negative population of the recipient BM cells (Fig. 7A) than in the whole BM (Fig. 7B). There were only 0.001% donor cells that displayed myelolymphoid lineage markers (Fig. 7B and C). Then we sorted CD45.2$^+$ mGS-derived cells from the BM of primary recipient mice (Fig. 7A) and injected 10^4 mGS-derived donor cells into the BM of irradiated secondary recipient NOD/SCIDγc^{null} mice. However, none of the host mice displayed donor-derived cells in the PB or BM after 4 months of the secondary transplantation. Thus, mGS-derived multipotent hematopoietic cells engrafted in the BM, but could not show stem cell potential by expanding and repopulating all the hematopoietic lineages posttransplantation for >16 weeks.

mGS-derived hematopoietic cells did not express CXCR4 or CDX4, but expressed HOXB4

Because mGS-derived hematopoietic cells did not engraft in the BM efficiently, we examined these cells for evidence of expression of a well-known and important homing receptor, CXCR4 (Fig. 8C). Indeed, very few mGS-derived CD45$^+$ cells expressed CXCR4. Also, c-kit expression was only 3% and the c-kit$^+$Sca-1$^+$ population represented only 0.09% of the culture elements. Because CDX4 and HOXB4 overexpression have enabled ES cells to engraft in vivo [2], the expression level of these genes was examined in mGS-derived cells using both RT-PCR and quantitative PCR. mGS-derived cells, as well as fetal liver and BM stem/progenitor cells, did not express mRNA for CDX4 (Fig. 8A). However, using the embryonic aorta-gonado-mesonephros (AGM) tissue as a reference (positive control tissue), the relative expression of HOXB4 in mGS-derived cells (0.76) was higher than embryonic day 16.5 fetal liver cells (0.02), BM lin$^-$ cells (0.09), BM Sca-1$^+$c-kit$^+$lin$^-$ cells (0.43), and CCE-derived cells (0.15) (Fig. 8B). From these results, it appears that the lack of CXCR4 expression of mGS-derived cells may be a primary reason that the transplanted cells could not expand in the recipient BM compartment.

Discussion

We report that multipotent hematopoietic progenitor cells are derived from mGS cells. mGS cells differentiate into Flk1$^+$ cells similar to differentiated ES cells. From mGS-derived Flk1$^+$ cells, erythroid, myeloid, lymphoid, and megakaryocyte hematopoietic progenitors were induced

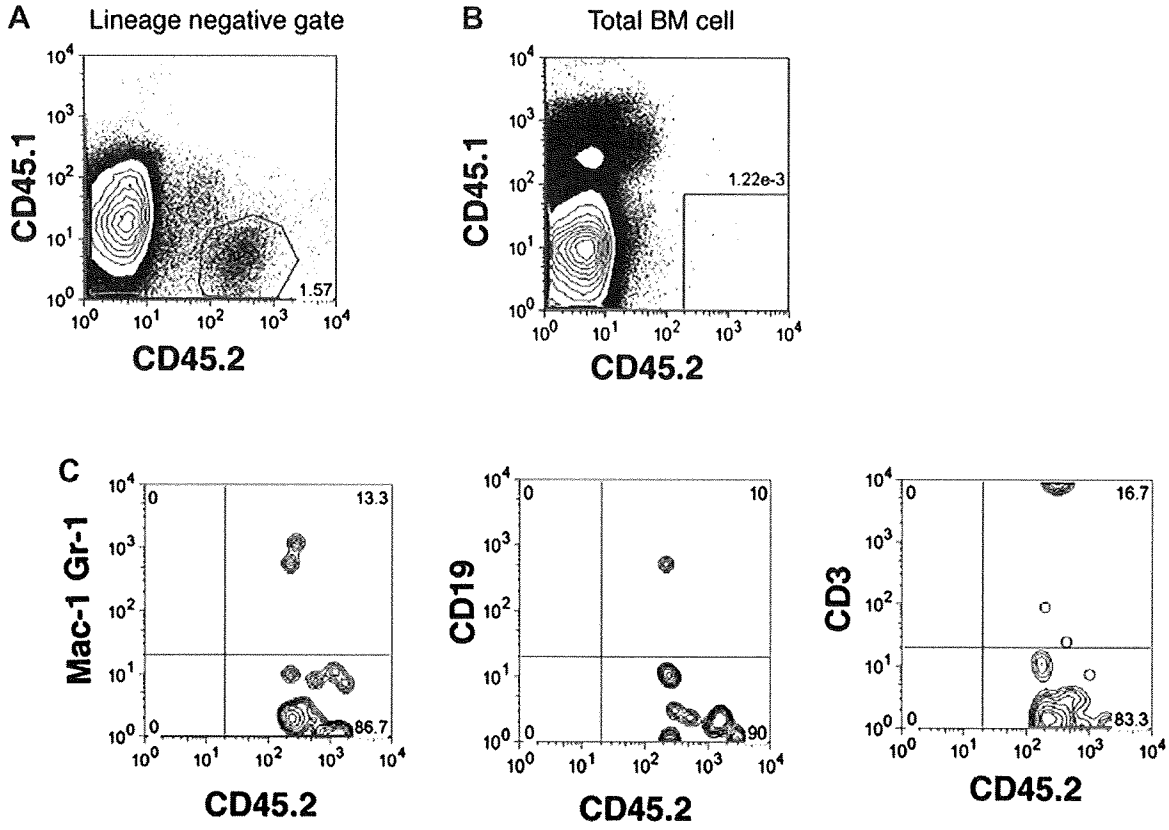

Figure 7. Analysis of primary recipient mice transplanted with mGS–derived hematopoietic cells. There are small percentages of mGS-derived cells in lineage negative fraction in the recipient bone marrow (BM) cells (**A**). When analyzing total recipient BM cells, mGS-derived cell can be detectable in very small percentage (**B**), but showed multi-lineage cell types (**C**).